International Journal of Numerical Methods for Heat and Fluid Flow

A comparative study of explicit high-resolution schemes for compositional simulations

Journal:	*International Journal of Numerical Methods for Heat and Fluid Flow*
Manuscript ID	HFF-08-2017-0333.R1
Manuscript Type:	Research Article
Keywords:	compositional, porous media, conservation laws, MUSCL, WENO, wave structure

Note: The following files were submitted by the author for peer review, but cannot be converted to PDF. You must view these files (e.g. movies) online.

Paper.tex

A comparative study of explicit high-resolution schemes for compositional simulations

October 31, 2017

Abstract

Purpose- In this paper, compositional flow of two- and three-phase fluids in one dimensional porous media is studied numerically and a comparison is made between several upwind and central numerical schemes.

Design/methodology/approach- Implicit Pressure Explicit Composition (IMPEC) procedure is used for discretization of governing equations. The pressure equation is solved implicitly while the mass conservation equations are solved explicitly using different Upwind (UPW) and Central (CEN) numerical schemes. These include Classical Upwind (UPW-CLS), Flux-based Decomposition Upwind (UPW-FLX), Variable-based Decomposition Upwind (UPW-VAR), Roe's Upwind (UPW-ROE), Local Lax Friedrichs (CEN-LLF), Dominant Wave (CEN-DW), Harten-Lax-van Leer (HLL), and newly proposed Modified Dominant Wave (CEN-MDW) schemes. To achieve higher resolution, high-order data generated by either MUSCL or WENO reconstructions are utilized.

Findings- It was found that the new CEN-MDW scheme can accurately solve multiphase compositional flow equations. This scheme utilizes most of the information in flux function while it has a moderate computational cost as a consequence of using simple algebraic formula for the wave speed approximation. Moreover, numerically calculated wave structure is shown to be used as a tool for a priori estimation of problematic regions, i.e., degenerate, umbilic, and elliptic points, which require to apply correction procedures to produce physically acceptable (entropy) solutions.

Research limitations/implications- This paper is concerned with one-dimensional study of compositional two- and three-phase flows in porous media. Temperature is assumed constant and the physical model accounts for miscibility and compressibility of fluids while gravity and capillary effects are neglected.

Practical implications- The proposed numerical scheme can be efficiently used for solving two- and three-phase compositional flows in porous media with a low computational cost which is especially useful when the number of chemical species increases.

Originality/value- A new central scheme is proposed that leads to improved accuracy and computational efficiency. Moreover, to the best of authors knowledge, this is the first time that the wave structure of compositional model is investigated numerically to determine the problematic situations during numerical solution and adopt appropriate correction techniques.

Keywords compositional, porous media, conservation laws, MUSCL, WENO, wave structure

Paper type Research paper

1 Introduction

Compositional model is one of the most comprehensive approaches for studying multi-component flow in hydrocarbon reservoirs (Cao, 2002; Orr, 2005; Han et al., 2006; Moortgat et al., 2012). This model can provide fairly accurate representation of hydrocarbon reservoir fluids (Firoozabadi, 1999; Haugen et al., 2007; Rezaveisi, 2015) using an Equation Of State (EOS) (Redlich and Kwong, 1949; Soave, 1972; Peng and Robinson, 1976). The mathematical formulation of compositional model usually consists of a parabolic pressure equation together with a system of hyperbolic mass conservation equations (Acs et al., 1985; Watts, 1986; Chen et al., 2006). The so-called Implicit Pressure Explicit Composition (IMPEC) approach is often used to solve the governing equations, in which the parabolic part is solved implicitly while the hyperbolic part is solved explicitly (Trangenstein and Bell, 1989; Coats, 2000). In one-dimensional case, the solution of pressure equation is usually obtained using Thomas algorithm (Conte and de Boor, 1980) while the solution of mass conservation equations requires much more efforts. This paper focuses on the latter part.

There are two different approaches for numerically solving hyperbolic conservation equations: 1) upwind, 2) central. To detect upwind direction, upwind schemes may use phase velocities (Thiele and Edwards, 2001; Mallison et al., 2005) or utilize characteristic decompositions together with an exact/approximate Riemann solver (Godunov, 1959; Roe, 1981; Bell et al., 1989; Edwards, 2005). The latter schemes usually exhibit good shock capturing properties; they are however, computationally expensive, especially for large systems of equations (Kurganov and Tadmor, 2000; Edwards, 2006, 2010) which is typical in compositional studies. On the other hand, central schemes with Rusanov-based flux approximations (Nessyahu and Tadmor, 1990; Liu et al., 2007) utilize one-wave approximation and eliminate the need for costly characteristic decomposition. These schemes may generate excessive numerical dissipation as they use the largest eigenvalue of the system to determine the one-wave speed. To alleviate this problem, the largest eigenvalue may be replaced by the so-called Dominant Wave (DW) (Edwards, 2006) speed. The DW scheme was successfully used for simulation of multi-phase flow in porous media using three-phase Buckley-Leverett and black-oil models (Moshiri et al., 2013).

Both upwind and central schemes are prone to numerical dissipation if they are implemented as first order methods. In order to reduce inherent numerical dissipation of these first order schemes, high-order reconstruction of variables can be used. This can be achieved using either Monotone Upstream-centered Schemes for Conservation Laws (MUSCL) methods (Van Leer, 1974; Sweby, 1984; Mallison et al., 2005) which utilize Total Variation Diminishing (TVD) concept or Weighted/-Essentially Non-Oscillatory (W/ENO) (Liu and Osher, 1998; Qiu and Shu, 2002; Christlieb et al., 2015) methods. In this work, both MUSCL and WENO reconstructions are used for simulation of the system of conservation laws. Extension of numerical schemes to high-order of accuracy in space is achieved in a simple straightforward way. Moreover, the computational cost of this extension will be relatively small if all extrapolations and limiting procedures are implemented in a component-wise manner.

To understand the mathematical properties of multi-component multi-phase flow, its wave structure should be studied. The wave structure of incompressible immiscible three phase flow, i.e, the Buckley-Leverett equations, has been studied extensively (Isaacson et al., 1992; Guzman and Fayers, 1997; Juanes and Patzek, 2004a). To account for the effect of fluid composition, the wave structure of compositional flow is investigated in this paper. This wave structure can be used to determine the problematic situations during numerical solution and adopt appropriate correction techniques.

Shocks and contact discontinuities frequently occur when solving hyperbolic system of equations. Numerical methods must therefore satisfy an appropriate entropy condition (Laney, 1998; Tadmor, 2003) for the solution to be admissible (Lax, 1973; Harten et al., 1976). Sometimes, upwind numerical schemes violate the entropy condition and exhibit non-physical features such as expansion shocks (Tadmor, 2003; Trangenstein, 2007). To obtain entropy satisfying solution, an appropriate correction (Harten et al., 1976; Tadmor, 1984; Kermani and Plett, 2001) may be used. Harten's correction (Harten and Hyman, 1983) has been used in the context of multi-component multi-phase

flow in porous media using black-oil model (Moshiri et al., 2013). Numerical experiments show that this correction is sensitive to its tuning parameter and may lead to over-diffusive solutions. Here, a different approach is used in which the flux of upwind scheme is substituted by a version of central flux at problematic points.

The objective of this paper is to assess the accuracy and computational cost of high-order upwind and central numerical schemes using the finite volume method. The context of this assessment is the system of mass conservation equations of compressible miscible multi-component multi-phase flow in porous media using compositional model.

In the following, first a brief review of the governing equations of compositional model is presented and the wave-structure of the system is investigated. Then, the numerical schemes for solving the system of conservation equations are described and the procedure to construct high-order schemes is presented. Finally, a number of benchmark problems are solved to assess the performance of different methods.

2 Compositional Model

In the compositional model used in this paper, reservoir temperature is considered constant and fluid is assumed to be consisted of n_c chemical components. Moreover, the fluid has at most $n_p = 3$ phases, i.e., liquid l, vapor v, and aqua a, while gravity and capillary effects are neglected.

Mole number of components is shown by vector $\mathbf{n}$ with n_c entities. Assuming thermodynamic equilibrium, components are distributed in phases, so that $\mathbf{n} = \mathbf{n}^l + \mathbf{n}^v + \mathbf{n}^a$, where $\mathbf{n}^\alpha$ is the vector of component mole numbers in phase α. Conservation of mass equation for ith component reads

$$\frac{\partial(\phi n_i)}{\partial t} = -\nabla \cdot \mathbf{v}_i + q_i, \qquad i = 1, 2, \cdots, n_c, \tag{1}$$

where ϕ is porosity and q_i is source/sink term of component i. Moreover, $\mathbf{v}_i$ is defined as,

$$\mathbf{v}_i = -\sum_{\alpha=1}^{n_p} x_i^\alpha \rho^\alpha f^\alpha m^{tot} \mathbf{K} \left(\nabla p + \varrho^\alpha g \nabla Z\right), \qquad i = 1, 2, \cdots, n_c, \tag{2}$$

where p is pressure and Z is reservoir altitude which is measured upward. In equation (2), $f^\alpha = \frac{m^\alpha}{m^{tot}}$ is fractional flow of phase α, while $m^{tot} = \sum_{\alpha=1}^{n_p} m^\alpha$ is total mobility in which, $m^\alpha = k_r^\alpha / \mu^\alpha$ is mobility of phase α where k_r^α and μ^α are relative permeability and viscosity of phase α, respectively. Moreover, x_i^α is mole fraction of component i in phase α, while ρ^α and ϱ^α are molar and mass densities of phase α, respectively. In addition, $\mathbf{K}$ is the tensor of rock absolute permeability and g is the gravitational acceleration.

Pressure equation is obtained using volume balance concept as

$$\phi(c_r + c_f)\frac{\partial p}{\partial t} = -\sum_{i=1}^{n_c} \nu_i^{tot} \nabla \cdot \mathbf{v}_i + \sum_{i=1}^{n_c} \nu_i^{tot} q_i, \tag{3}$$

where c_r and c_f are rock and fluid compressibilities, respectively. Moreover, ν_i^{tot} is total partial molar volume of ith component which is calculated based on EOS and PVT relations. For further discussion on the formulation the reader is referred to (Hoteit and Firoozabadi, 2006). The present paper utilizes SI units.

In this work, an IMPEC approach is used to solve the fluid flow equations. In this approach, using the given temperature, pressure, and composition $\mathbf{n}$ at time t, first a stability analysis (Michelsen, 1982a; Nelson, 1987; Iranshahr et al., 2010) is performed to specify the number of phases existing at each cell in the reservoir. If multiple phases are present, flash calculations (Michelsen, 1982b; Pan and Firoozabadi, 2003; Michelsen et al., 2008) should be performed to determine the distribution of components in each phase, i.e., $\mathbf{n}^\alpha$. The procedures for calculating thermodynamic equilibrium and fluid properties, e.g. ρ^α, ϱ^α, and s^α, can be found in (Firoozabadi,

1999; Whitson and Brulé, 2000; Michelsen et al., 2008). To calculate hydrocarbon phase viscosities μ^α, an algorithm proposed by Lohrenz et al. (1964) is used. Moreover, relative permeabilities k_r^α are considered to be a function of phase saturation s^α. Using fluid properties, at each time step, pressure equation (3) is solved implicitly while its coefficients are calculated using compositions at present time step. Then, using this pressure field, the system of mass conservation equations (1) is solved explicitly. Solution of these equations is of main concern in this paper and will be discussed in detail later.

In section 3, first the mathematical (or wave) structure of conservation equations (1) is studied in detail in order to understand how the physical complexities of the compositional model lead to mathematical complexities of the hyperbolic system of equation to be solved.

3 Wave Structure

The system of mass conservation equations of multi-component multi-phase flow in porous media has a complex mathematical structure that may contain umbilic and/or elliptic regions (Guzman and Fayers, 1997; Juanes and Patzek, 2004a), for example in three-phase Buckley-Leverett equations, where compressibility and miscibility effects are neglected, it has been known that, gravitational forces together with relative permeability and viscosity ratio of phases may generate umbilic and/or elliptic regions (Trangenstein, 1989; Holden, 1990; Isaacson et al., 1992; Guzman and Fayers, 1997; Marchesin and Plohr, 2001; Juanes and Patzek, 2004b). Here, the mathematical (wave) structure of compressible miscible multi-component two-phase system of conservation laws appearing in a compositional model is studied and the parameters affecting the wave structure are discussed. For the sake of simplicity, and without loss of generality, it is assumed that the fluid consists of three components, so ternary diagrams can be used for visual demonstration. Clearly, the discussion in this section is not limited to three-component systems.

Ternary diagrams are used extensively in petroleum industry to analyze properties and phase behavior of three-component fluids (Mccain, 1990; Johns and Orr, 1996). Figure 1a shows a typical ternary phase diagram for a compositional problem for which the fluid and PVT properties are given in Tables 1 and 2, respectively. Phase behavior is calculated at average pressure, i.e. $p = \frac{p_{inj}+p_{prd}}{2}$. Each side of triangle represents molar composition, z_i, of one component. Based on the relation $\sum_{i=1}^{n_c} z_i = 1$, all possible composition states lie within the triangle. The components are assigned to triangle corners from lighter to heavier molecular weight in a clock-wise manner with the lightest component located at the top. Depending on composition, temperature, pressure, and the selected EOS, fluid at any point in the ternary diagram can be either single or two-phase. In Figure 1a different phase regions are seen.

Table 1: Problem properties

Components	C_1	C_2	C_3
Injection mole fraction [-]	0.90	0.10	0.00
Initial mole fraction [-]	0.00	0.25	0.75
Initial pressure [MPa]	6.9		
Injection pressure [MPa]	7.0		
Temperature [K]	311		
Porosity [-]	0.2		
Permeability [mD]	10		
Relative permeability [-]	$k_r^\alpha = s^\alpha$		

Besides phase behavior, ternary diagrams can be used to describe the mathematical structure of the system of hyperbolic conservation laws governing three-component two-phase compositional flow, i.e. equation (1). To begin with, the system of conservation equations (1) is written in its

Table 2: PVT properties of components (Danesh, 1998)

Components	Symbol	p_c [MPa]	T_c [K]	Z_c [-]	M_w [kg/kg-mol]	ω [-]
Methane	C_1	4.599	190.56	0.2862	16.043	0.0115
Ethane	C_2	4.873	305.32	0.2793	30.070	0.0995
Propane	C_3	4.248	369.83	0.2763	44.096	0.1523

quasi-linear form,

$$\frac{\partial \mathbf{n}}{\partial t} + \mathbf{J}\frac{\partial \mathbf{n}}{\partial x} = \mathbf{0}, \tag{4}$$

where $\mathbf{J} = \frac{\partial \mathbf{f}}{\partial \mathbf{n}}$ is the Jacobian matrix. Moreover, $\lambda_1 \leq \lambda_2 \leq \lambda_3$ are eigenvalues of this matrix, while $\mathbf{r}_1, \mathbf{r}_2, \mathbf{r}_3$ are the corresponding eigenvectors. To be consistent with the formulation given in the previous section, investigation is based on the assumption of IMPEC procedure where pressure p and total velocity v^{tot} are considered constant, i.e., independent of $\mathbf{n}$, when conservation equations are to be solved. In Figures 1b to 1d, eigenvalues of the system of Tables 1 and 2 are shown. Solution of the system of hyperbolic conservation equations involves n_c individual waves that connect two separate states known as the left and right states. The eigenvalues of hyperbolic system are in fact the speeds of waves traveling in composition space. So, Figures 1b to 1d represent the wave structure of the system as well. It can be seen from Figure 1 that at some points the wave speeds show unexpected abnormalities. These composition states are mainly located near binodal curve that separates one- and two-phase regions. This implies a dramatic variation in wave structure during phase change process. As shown in Figures 1b to 1d, the fastest wave speed λ_3 varies mainly along bubble-point curve where its maximum values located while the intermediate wave speed λ_2 changes considerably along dew-point curve. An interesting fact about the intermediate wave speed λ_2 and the fastest wave speed λ_3 is that they remain approximately the same and equal to $\rho^{\alpha} v^{tot}$ in single phase region, where ρ^{α} refers to single phase molar density; However, in the two-phase region λ_2 and λ_3 behave quite differently. On the other hand, the slowest wave speed λ_1 is almost zero everywhere in the composition space which is in agreement with the findings of (Trangenstein and Bell, 1989). Of course, some relatively small variations, with respect to other λ_is, exist as a consequence of numerical differentiation.

It must be noted that when Buckley-Leverett equations are studied, the eigen-structure can be obtained analytically (Juanes and Patzek, 2004a). However, in a compositional model, the relation between flux functions $\mathbf{f}$ and the composition $\mathbf{n}$ is so complex that the Jacobian and its eigen-structure should be evaluated numerically. If some simplifying assumptions are made, finding analytical solutions in the form of Method Of Characteristic (MOC) for compositional problems will be possible (Falls and Schulte, 1992; Jessen et al., 2001; Orr, 2005; LaForce et al., 2008b). More specifically, a key concept in wave structure and analytical solutions of two phase compositional flow is the so-called tie-line which connects compositions of liquid and vapor phases in equilibrium. Each point on a tie line represents a composition in the two-phase region, hence, along a tie line the phase compositions are fixed while the saturations of phases vary (LaForce et al., 2006). The MOC solutions show that only a few (key) tie-lines determine the structure of the solution route in composition space (Jessen et al., 2001; LaForce et al., 2006). The MOC theory has been recently extended to three-phase flows (LaForce et al., 2008b). In this section, no simplifying assumption is made and the wave structure is obtained numerically. In section 5, the MOC solutions are utilized for validation of numerical procedures.

In order to further study mathematical properties of the system, the so-called structural non-linearity coefficients are defined as $\kappa_{ii} = \nabla\lambda_i \cdot \mathbf{r}_i$, where ∇ is evaluated with respect to $\mathbf{n}$ (Bell et al., 1989). κ_{ii}s resemble second derivatives for a scalar variable and can be used to measure the non-linearity of the system. Specifically, $\kappa_{ii} \neq 0$ indicates that the system is genuinely non-linear (convex in scalar case) and $\kappa_{ii} = 0$ shows that the system is linearly degenerate (non-convex in scalar case). It is noteworthy that, in this context, the term convexity is defined to be the opposite

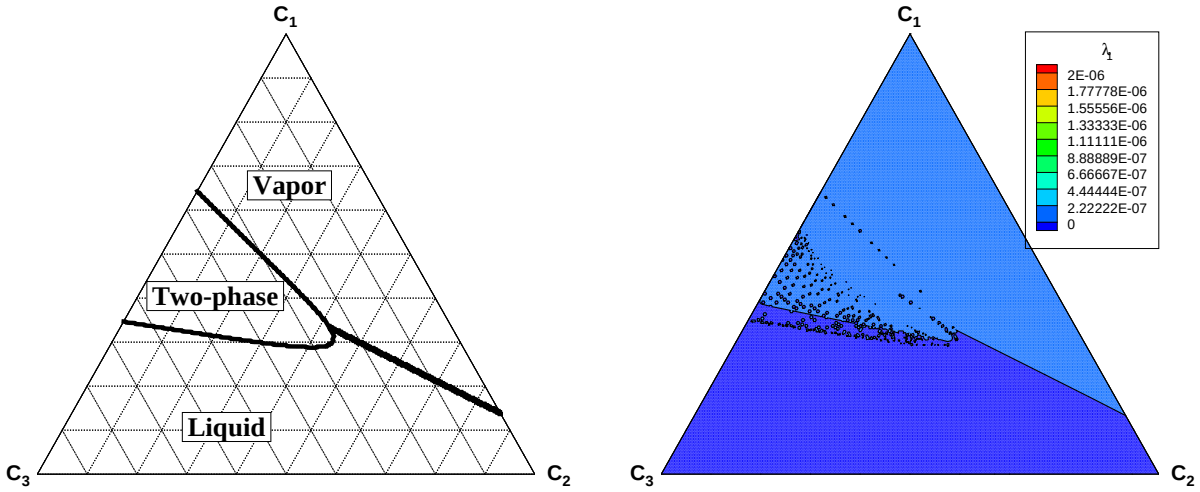

(a) Fluid phase behavior

(b) λ_1

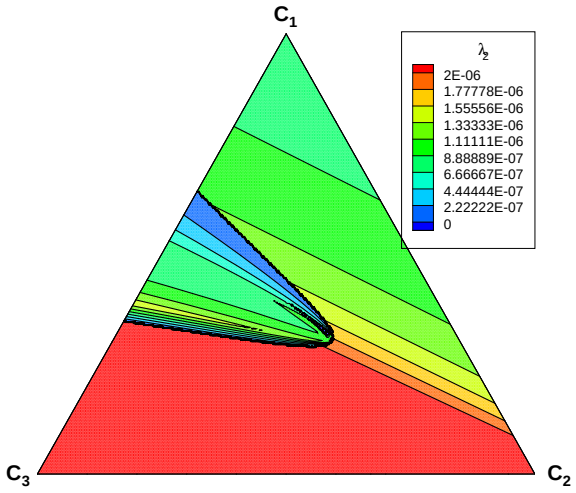

(c) λ_2

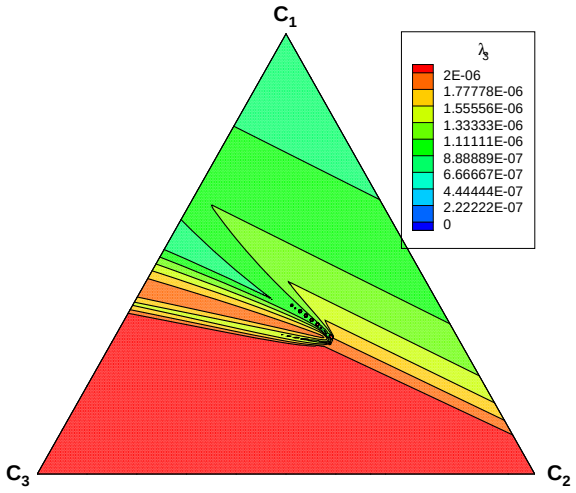

(d) λ_3

Figure 1: Phase behavior and wave structure ($\lambda_1 \leq \lambda_2 \leq \lambda_3$) of the system of Table 1

of linearity and so includes concavity as well. Figures 2a to 2c show the genuinely nonlinear states, i.e., $\kappa_{ii} \neq 0$, within the composition space for each wave family. It should be noted that the 1st wave family is linearly degenerate everywhere due to the fact that $\lambda_1 = 0$. On the other hand, the 2nd and 3rd wave families are linearly degenerate in single phase region which is consistent with (Trangenstein and Bell, 1989). It should be noted that, since the derivatives in κ_{ii} are calculated numerically $\kappa_{ii} = 0$ cannot be obtained exactly due to numerical errors. These figures imply that, the system in hand is neither entirely genuinely non-linear nor linearly degenerate; in fact in the most of composition states the system is linearly degenerate, while in some points the system is non-linear. Such systems are sometimes called non-genuinely non-linear (Dicks, 1993). In a linearly degenerate system, compound waves, for example a wave consisting of both rarefaction and shock, may occur (Dicks, 1993).

Another problem in solving hyperbolic system of conservation laws arises when the system loses its strict hyperbolicity. This occurs when in a composition state two or more eigenvalues (wave speeds) become equal. Such composition states are called umbilic points (Dicks, 1993). In some cases umbilic points are close to each other and generate umbilic regions in composition space. De-

ficiency of eigenvector bases or the so-called parabolic degeneracy may occur at umbilic points, i.e. some of eigenvectors may not be determined independently. Because of this eigenvector deficiency, the schemes using characteristic decomposition cannot be implemented successfully at such points. Moreover, at umbilic points the waves can be transformed from one family to another (Lax, 1973; Liu, 1975; Dicks, 1993). As opposed to strictly hyperbolic systems where constant left and right states are connected by only simple waves, i.e. one rarefaction or one shock. Figure 2d shows umbilic points for the current problem. It is evident that all single phase states are essentially umbilic points due to the equality of λ_2 and λ_3 in this region. Moreover, there are some umbilic points within two phase regions.

The most severe situation for a hyperbolic system occurs when at some composition states complex eigenvalues appear. Such points lead to elliptic regions within the hyperbolic composition space. In theory, it is difficult to solve such hyperbolic-elliptic coupled system, because boundary conditions should be applied on all boundaries of elliptic region at each time (Isaacson et al., 1988, 1992; Guzman and Fayers, 1997). However, in practice, when these elliptic regions are confined and of relatively small size, they can be disregarded by some corrections in numerical schemes in the expense of additional numerical diffusion. In particular, omitting the imaginary parts of complex conjugate eigenvalues leads to umbilic points which, in turn, makes the use of non-decomposition schemes inevitable. Present numerical investigation, in accordance with other analytical studies (Trangenstein and Bell, 1989; Orr, 2005), shows that two phase flows such as introduced in Tables 1 and 2 do not generate elliptic points. In fact, the current study confirms that this sort of problematic points belongs only to special cases in three phase flows as a consequence of relative permeability models and/or gravitational forces, as it is shown already in (Guzman and Fayers, 1997).

It is worth mentioning that the sorting of λ_is does not affect the studies here as long as the correspondent columns of eigenvector matrix are sorted accordingly. The same is true when these eigen-structures are used in upwind numerical schemes in which the sorting of λ_is does not affect the characteristic decomposition. However, these sorted λ_is may not correspond to the same wave family over the entire composition domain. In fact, the loss of strict hyperbolicity can be an indication of the change in the order of eigenvalues.

Ternary wave structures as depicted in this section, can be used as a tool for choosing appropriate numerical schemes for each problem. As mentioned before, there are a large number of possibilities for methods of solving a hyperbolic system of equations. However, for all schemes, it is necessary to use a procedure to detect problematic regions, i.e., degenerate, umbilic, and elliptic points, and apply corrections to produce physically acceptable (entropy) solutions (Tadmor, 2003; Juanes and Patzek, 2004a). However, these detection procedures are relatively complex and time consuming because they should be applied to each composition state at each time step. It is recommended that, the wave structure as shown in this section should be calculated prior to using the marching procedure and only if problematic regions exist within composition domain, correction procedures are applied.

It is worth mentioning that, when the wave structure calculations are performed numerically it is possible in some cases that the numerical differentiation leads to false detection of problematic points or fails to detect some valid problematic points. The situation can be mitigated by adjusting the variations (δ) and tolerances (ϵ) of numerical calculations. Table 3 presents the tolerances used for the calculations of this section and can be used for similar compositional wave structure calculations. Moreover, even if the computed problematic points do not conform exactly with the physics, they surely exhibit problematic behavior in numerical schemes where all the computations are performed numerically.

Nevertheless, the analysis of wave structure in this section indicates that the numerical differentiation can be used as a tool for a priori estimation of mathematical behavior of the system of conservation equations in hand, despite its flux function complexities. As it is stated earlier, the analysis of this section is not limited to three-component systems and can be used with arbitrary number of equations as well but graphical visualization will be more difficult.

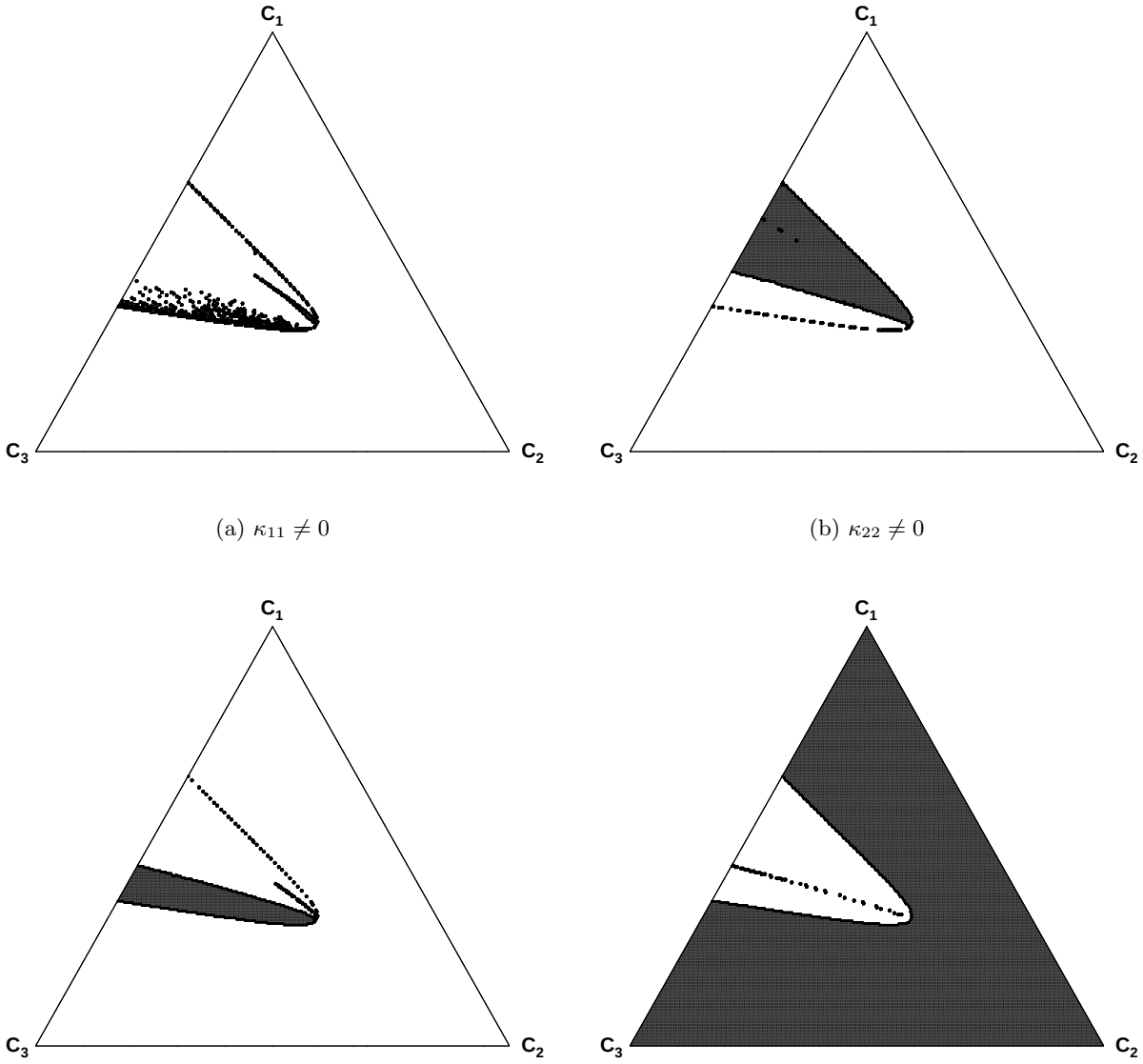

(a) $\kappa_{11} \neq 0$ (b) $\kappa_{22} \neq 0$

(c) $\kappa_{33} \neq 0$ (d) Umbilic points

Figure 2: Genuinely nonlinear and umbilic points in wave-structure

Table 3: Tolerances for numerical wave structure calculations

δn	$\epsilon_{degenerate}$	$\epsilon_{umbilic}$	$\epsilon_{elliptic}$
1.0×10^{-3}	1.0×10^{-5}	$1.0 \times 10^{-2} \left(\max_{k=1}^{n_c} \lvert\lambda_k\rvert \right)$	$1.0 \times 10^{-3} \left(\max_{k=1}^{n_c} \lvert\lambda_k\rvert \right)$

4 Numerical Method

4.1 Discretization of Equations

A finite volume approach is used for the discretization of equations (1) and (3). In one-dimension, position of grid points is defined as

$$x_j = (j-1)\triangle x, \qquad j = 1, 2, \cdots, N, \tag{5}$$

where $\triangle x$ and N are cell length and the total number of cells, respectively. Moreover, A_j is the cross section area of cell j. Assuming $(\triangle x)_{j\pm1/2} = (\triangle x)_j = \triangle x$ and $A_{j\pm1/2} = A_j = A$ and define

$$\xi_{j\pm1/2} = \frac{K}{\triangle x}\left(\sum_{i=1}^{n_c}\nu_i^{tot}\sum_{\alpha=1}^{n_p}x_i^\alpha\rho^\alpha f^\alpha m^{tot}\right)_{j\pm1/2} \tag{6a}$$

and

$$\eta_{j\pm1/2} = \frac{K}{\triangle x}\left(\sum_{i=1}^{n_c}\nu_i^{tot}\sum_{\alpha=1}^{n_p}x_i^\alpha\rho^\alpha f^\alpha m^{tot}\varrho^\alpha\right)_{j\pm1/2} g\sin\theta \tag{6b}$$

where θ is defined in Figure 4. The discretized form of pressure equation (3) becomes:

$$\frac{\triangle x}{\triangle t}\left[\phi_j(c_{rj}+c_{fj})+\xi_{j+1/2}+\xi_{j-1/2}\right]p_j^{n+1}-\xi_{j+1/2}p_{j+1}^{n+1}-\xi_{j-1/2}p_{j-1}^{n+1} = \frac{\triangle x}{\triangle t}\phi_j(c_{rj}+c_{fj})p_j^n+\eta_{j+1/2}-\eta_{j-1/2} \tag{7}$$

Harmonic averaging is used to find the discrete coefficients at cell interfaces (Chen et al., 2006).

The semi-discrete form of the mass conservation equations (1) is given by

$$\frac{d}{dt}(\mathbf{n}_j) = -\frac{1}{\phi_i\Delta x}\left(\hat{\mathbf{f}}_{j+1/2}^n-\hat{\mathbf{f}}_{j-1/2}^n\right), \tag{8}$$

where $\hat{\mathbf{f}}_{j\pm1/2}^n = \hat{\mathbf{f}}(\mathbf{f}_L,\mathbf{f}_R)_{j\pm1/2}^n$ is the vector of components numerical flux calculated at interfaces $j\pm1/2$, in which

$$\mathbf{f}_{L,R} = \sum_{\alpha=1}^{n_p}\mathbf{f}_{L,R}^\alpha = \frac{KA}{\triangle x}\left[\sum_{\alpha=1}^{n_p}\mathbf{x}^\alpha\rho^\alpha f^\alpha m^{tot}\left(\triangle p+\varrho^\alpha g\triangle x\sin\theta\right)\right]_{L,R}, \tag{9}$$

and $\triangle p \equiv \pm(p_{j\pm1}-p_j)$.

To study fluid flow in one-dimensional reservoirs using the compositional model, the pressure equation (7) must be solved along with the conservation equations (8). The resulting tridiagonal linear system of equations given by (7) can be easily solved using Thomas algorithm (Conte and de Boor, 1980). The rest of this section is dedicated to solving conservation equations (8). To solve equations (8) it is necessary to approximate numerical fluxes $\hat{\mathbf{f}}_{j\pm\frac{1}{2}}$. In this paper, several upwind and central schemes are used for this purpose. Hereafter, the face subscript $j\pm\frac{1}{2}$ is omitted for brevity.

4.2 Classical Upwind Scheme

The simplest scheme used for solving the conservation equations (8) is the classical upwind scheme (UPW-CLS) which is widely used in petroleum reservoir simulators. In this scheme, the numerical flux function $\hat{\mathbf{f}}$ in equation (8) is computed based on the sign of phase flux as (Aziz and Settari, 1979)

$$\hat{\mathbf{f}} = \sum_{\alpha=1}^{n_p}\mathbf{f}^\alpha = \sum_{\alpha=1}^{n_p}\left[\frac{\max(\omega^\alpha,0)}{|\omega^\alpha|}\mathbf{f}_L^\alpha-\frac{\min(\omega^\alpha,0)}{|\omega^\alpha|}\mathbf{f}_R^\alpha\right], \tag{10}$$

where $\mathbf{f}_L = \mathbf{f}(\mathbf{n}_L)$ and $\mathbf{f}_R = \mathbf{f}(\mathbf{n}_R)$ are flux functions calculated at the left and right cell interface states, i.e., $\mathbf{n}_L$ and $\mathbf{n}_R$, respectively using (9). Moreover, the so-called potential difference is defined as $\omega^\alpha = p_L^\alpha+\varrho_L^\alpha gZ_L-p_R^\alpha-\varrho_R^\alpha gZ_R$ which is simplified in the absence of capillary and gravity effects to $\omega^\alpha = p_L-p_R$. In such cases, the scheme of (10) is equivalent to component-wise flux $\hat{\mathbf{f}} = \mathbf{f}_L$ or $\hat{\mathbf{f}} = \mathbf{f}_R$ depending on the sign of pressure gradient. In fact, (10) is a flux splitting scheme based on physical concept of phase flow. This scheme is implemented efficiently since there is no need for characteristic decomposition or any other eigen-structure calculation.

4.3 Flux-based Decomposition Upwind Scheme

In order to obtain a flux-based upwind scheme, all wave directions may be detected through characteristic decomposition as,

$$\hat{\mathbf{f}} = \frac{1}{2}\left(\mathbf{f}_R + \mathbf{f}_L\right) - \frac{1}{2}\mathbf{R}\,\mathbf{sgn}(\mathbf{\Lambda})\mathbf{R}^{-1}\left(\mathbf{f}_R - \mathbf{f}_L\right), \tag{11}$$

where $\mathbf{sgn}(\mathbf{\Lambda}) \equiv \mathrm{diag}(\mathrm{sgn}(\lambda_1), \mathrm{sgn}(\lambda_2), \cdots, \mathrm{sgn}(\lambda_{n_c}))$ while λ_j is the jth eigenvalue and $\mathbf{R} = [\mathbf{r}_1, \mathbf{r}_2, \cdots, \mathbf{r}_{n_c}]$ is the matrix of right eigenvectors of the Jacobian matrix $\frac{\partial \mathbf{f}}{\partial \mathbf{n}}$ evaluated at $\mathbf{n}_M = \frac{\mathbf{n}_L + \mathbf{n}_R}{2}$. The scheme of equation (11) is named UPW-FLX hereafter. This scheme is clearly computationally expensive.

4.4 Variable-based Decomposition Upwind Scheme

The scheme of equation (11) can be rewrite in variable format as

$$\hat{\mathbf{f}} = \mathbf{f}\left[\frac{1}{2}\left(\mathbf{n}_R + \mathbf{n}_L\right) - \frac{1}{2}\mathbf{R}\,\mathbf{sgn}(\mathbf{\Lambda})\mathbf{R}^{-1}\left(\mathbf{n}_R - \mathbf{n}_L\right)\right], \tag{12}$$

which is called UPW-VAR hereafter.

4.5 Roe-based Upwind Scheme

Alternatively, one can define upwind numerical flux as,

$$\hat{\mathbf{f}} = \frac{1}{2}\left(\mathbf{f}_R + \mathbf{f}_L\right) - \frac{1}{2}\mathbf{R}\,|\mathbf{\Lambda}|\,\mathbf{R}^{-1}\left(\mathbf{n}_R - \mathbf{n}_L\right), \tag{13}$$

where $\mathbf{\Lambda} \equiv \mathrm{diag}(\lambda_1, \lambda_2, \cdots, \lambda_{n_c})$. The scheme of (13) is a modification of Roe's upwind scheme (Bell et al., 1989) and is called UPW-ROE in this paper.

It should be noted that, in order to use the UPW-FLX, UPW-VAR, or UPW-ROE schemes, it is necessary to have a set of independent eigenvector bases so that $\mathbf{R}^{-1}$ can be calculated, otherwise at the umbilic points with eigenvector deficiency the schemes fail to predict correct solution. To deal with such points, relatively complicated procedures have been proposed (Bell et al., 1989; Edwards, 2010). However, in this paper a simple approach as described in section 4.12 is implemented to circumvent this problem.

4.6 Harten-Lax-van Leer Scheme

Harten-Lax-van Leer (HLL) is a two-wave scheme that computationally lies between decomposition upwind schemes as prescribed above and one-wave central schemes as discussed later. The numerical flux is defined as,

$$\hat{\mathbf{f}} = \begin{cases} \mathbf{f}_L & \tilde{\lambda}_L \geq 0, \\ \dfrac{\tilde{\lambda}_R \mathbf{f}_L - \tilde{\lambda}_L \mathbf{f}_R + \tilde{\lambda}_L \tilde{\lambda}_R \left(\mathbf{n}_R - \mathbf{n}_L\right)}{\tilde{\lambda}_R - \tilde{\lambda}_L} & \tilde{\lambda}_L < 0 < \tilde{\lambda}_R, \\ \mathbf{f}_R & \tilde{\lambda}_R \leq 0. \end{cases} \tag{14}$$

The so-called signal speeds $\tilde{\lambda}_L$ and $\tilde{\lambda}_R$ are originally introduced for solving Euler equations of gas dynamics (Toro, 2009); however, for other systems they can be generalized to $\tilde{\lambda}_L = \min(\lambda_L^{min}, \lambda_M^{min})$ and $\tilde{\lambda}_R = \max(\lambda_M^{max}, \lambda_R^{max})$, where $\lambda_\beta^{max} = \max_{i=1}^{n_c}(\lambda_{i,\beta})$ and $\lambda_\beta^{min} = \min_{i=1}^{n_c}(\lambda_{i,\beta})$ for $\beta = L, M, R$ (Trangenstein, 2007).

4.7 Local Lax-Friedrichs Scheme

To avoid the costly characteristic decomposition and the need for a set of independent eigenvectors as in UPW-FLX, UPW-VAR, and UPW-ROE schemes, the so-called central schemes can be employed. Local Lax-Friedrichs (CEN-LLF) scheme lies in this category for which the numerical flux function is defined as (Liu and Osher, 1998; Edwards, 2010)

$$\hat{\mathbf{f}} = \frac{1}{2}\left(\mathbf{f}_R + \mathbf{f}_L\right) - \frac{1}{2}\left|\lambda_{LLF}\right| \mathbf{I}\left(\mathbf{n}_R - \mathbf{n}_L\right), \tag{15}$$

where the CEN-LLF wave speed (λ_{LLF}) is approximated as (Edwards, 2010)

$$\left|\lambda_{LLF}\right| = \max_{[x_L, x_R]} \left(\max_{i=1}^{n_c} \left|\lambda_i\right| \right) \cong \max\left(|\lambda_L^{\max}|, |\lambda_{GL}^{\max}|, |\lambda_M^{\max}|, |\lambda_{GR}^{\max}|, |\lambda_R^{\max}|\right). \tag{16}$$

Here $\lambda_L^{\max}$, $\lambda_R^{\max}$, and $\lambda_M^{\max}$ are the maximum eigenvalues corresponding to the Left, Right, and Mean values and are calculated at $\mathbf{n}_L$, $\mathbf{n}_R$, and $\mathbf{n}_M = (\mathbf{n}_L + \mathbf{n}_R)/2$, respectively. Moreover, $\lambda_{GL}^{\max}$ and $\lambda_{GR}^{\max}$ are the maximum eigenvalues corresponding to Left and Right Gauss points calculated at $\mathbf{n}_{GL} = \mathbf{n}_M + (\mathbf{n}_L - \mathbf{n}_M)/\sqrt{3}$ and $\mathbf{n}_{GR} = \mathbf{n}_M + (\mathbf{n}_R - \mathbf{n}_M)/\sqrt{3}$, respectively. Comparing (15) and (13) it can be inferred that the term $\mathbf{R}\left|\mathbf{\Lambda}\right|\mathbf{R}^{-1}$ is approximated by $\left|\lambda_{LLF}\right|\mathbf{I}$ in the CEN-LLF scheme.

4.8 Dominant Wave Scheme

While the scheme defined by (15) is decomposition free, it is still complicated and several eigen-structures should be evaluated at each interface. The Dominant Wave (CEN-DW) scheme alleviates this problem by defining the numerical flux as

$$\hat{\mathbf{f}} = \frac{1}{2}\left(\mathbf{f}_R + \mathbf{f}_L\right) - \frac{1}{2}\left|\lambda_{DW}\right| \mathbf{I}\left(\mathbf{n}_R - \mathbf{n}_L\right), \tag{17}$$

where the CEN-DW speed (λ_{DW}) is defined as (Edwards, 2006)

$$\lambda_{DW} = \frac{\left(\mathbf{n}_R - \mathbf{n}_L\right) \cdot \left(\mathbf{f}_R - \mathbf{f}_L\right)}{\left(\mathbf{n}_R - \mathbf{n}_L\right) \cdot \left(\mathbf{n}_R - \mathbf{n}_L\right)}. \tag{18}$$

This speed is consistent with the Rankine-Hugoniot shock relation (Trangenstein, 2007) and has successfully been used in conjunction with the Enquist-Osher (Bell et al., 1989; Chen et al., 1992) flux calculation. The main advantage of using the dominant wave speed as defined in (18) is that there is no need for eigen-structure evaluation. For further discussions on this consult (Edwards, 2006; Moshiri et al., 2013).

4.9 Modified Dominant Wave Scheme

The CEN-DW scheme, despite its simplicity and cost efficiency, depends only on L and R states and information in the region (L, R) is excluded in the formulation. This is especially crucial, when the flux function is complicated between L and R, for example when non-convexities exist in the form of local extrema. To overcome this deficiency while maintaining the simplicity of aforementioned scheme, Modified Dominant Wave (CEN-MDW) scheme is presented here that incorporates the basis of both CEN-LLF and CEN-DW. In particular, the numerical flux of this new scheme is defined as,

$$\hat{\mathbf{f}} = \frac{1}{2}\left(\mathbf{f}_R + \mathbf{f}_L\right) - \frac{1}{2}\left|\lambda_{MDW}\right| \mathbf{I}\left(\mathbf{n}_R - \mathbf{n}_L\right), \tag{19}$$

where the CEN-MDW wave speed (λ_{MDW}) is defined as

$$|\lambda_{MDW}| = \max(|\bar{\lambda}_{L-GL}|, |\bar{\lambda}_{GL-M}|, |\bar{\lambda}_{M-GR}|, |\bar{\lambda}_{GR-R}|), \tag{20}$$

with

$$\bar{\lambda}_{1-2} = \frac{\left(\mathbf{n}_2 - \mathbf{n}_1\right) \cdot \left(\mathbf{f}_2 - \mathbf{f}_1\right)}{\left(\mathbf{n}_2 - \mathbf{n}_1\right) \cdot \left(\mathbf{n}_2 - \mathbf{n}_1\right)}. \tag{21}$$

The latter scheme has the advantage of not being prone to entropy violating solutions while the added computational cost is relatively small.

4.10 Some Comments on Central Schemes

As it can be seen from equations (15), (17), and (19) all CEN-LLF, CEN-DW, and CEN-MDW schemes use a one-wave approximation for wave speed, i.e., all waves propagate with the same speed. Although in reality this is not the case, but if wave speed is approximated accurately, the numerical flux will be consistent with the physical flux except for some additional dissipation.

LLF scheme considers a conservative approach towards wave speed approximation and assumes that all waves travel with the largest speed computed at a face. This results in better stability but higher numerical dissipation for a given time step size since the one-wave speed works similar to artificial dissipation (Tadmor, 1984, 2003). Because of this additional diffusion, the CEN-LLF scheme shows better stability and smaller oscillations when encountering problematic regions compared to upwind schemes for the same CFL number.

In contrast to CEN-LLF, the CEN-DW scheme considers a severe approach towards the one-wave speed calculation and utilizes a simple formula to find out a less dissipative wave speed. As expected, the CEN-DW speed usually lies below the CEN-LLF wave speed. This leads to far less dissipation and larger time step size as the time step is inversely proportional to the wave speed. However, the latter scheme just use the information in n_L and n_R states and neglect other information.

On the other hand, the proposed scheme (CEN-MDW) uses a more practical approach for calculation of one-wave speed as it utilizes the maximum of dominant speeds for each interface and includes the information of flux function in the region $[n_L, n_R]$.

Figure 3 schematically compares the procedures for one-way speed approximation in CEN-LLF, CEN-DW, and CEN-MDW schemes. Figure 3a shows a typical flux of a scalar conservation equation as a function of $n \in [n_L, n_R]$. When CEN-LLF scheme is used, the region between n_L and n_R is divided into four subregions and the maximum of eigenvalues (flux derivative in scalar case) is assigned as wave speed at the corners of these subregions, as shown in Figure 3b. Finally the maximum of these speeds is selected as CEN-LLF wave speed in (15). When CEN-DW scheme is used, the flux is approximated linearly in the region $[n_L, n_R]$ and the wave speed is equal to the slope of the line connecting n_L and n_R, as shown in Figure 3c. When using CEN-MDW scheme, as shown in Figure 3d, the region between n_L and n_R is divided into four subregions and in each subregion the physical flux is approximated linearly using a two-point central scheme to obtain the slopes given by (21). Then, the maximum of these slopes is used to approximate the numerical flux (19). Computational cost of this new approach is much smaller than that of (15) and it is very unlikely to generate expansion shocks since it rarely produce near zero wave speeds.

4.11 High-order States

For a first-order scheme, the left and right states in equations (10), (11), (12), (13), (14), (15), (17) and (19) are simply the values of neighboring nodes of each interface, i.e. the values at j and $j+1$ are used as the left L and right R states, respectively for interface $j+1/2$. In the following, two procedures are described to reconstruct high-order states. Here, the study is limited to the second-order schemes.

4.11.1 MUSCL Reconstruction

In order to provide a high-order scheme with TVD properties, one can define L and R states using a MUSCL reconstruction (Lyra and Morgan, 2000). This is applied to each component of vector $\mathbf{n}$ shown here by a typical scalar variable n as (Hirsch, 2007)

$$n_L = n_j + \frac{1}{2}\phi(r^+)(n_{j+1} - n_j), \tag{22a}$$

$$n_R = n_{j+1} - \frac{1}{2}\phi(r^-)(n_{j+1} - n_j), \tag{22b}$$

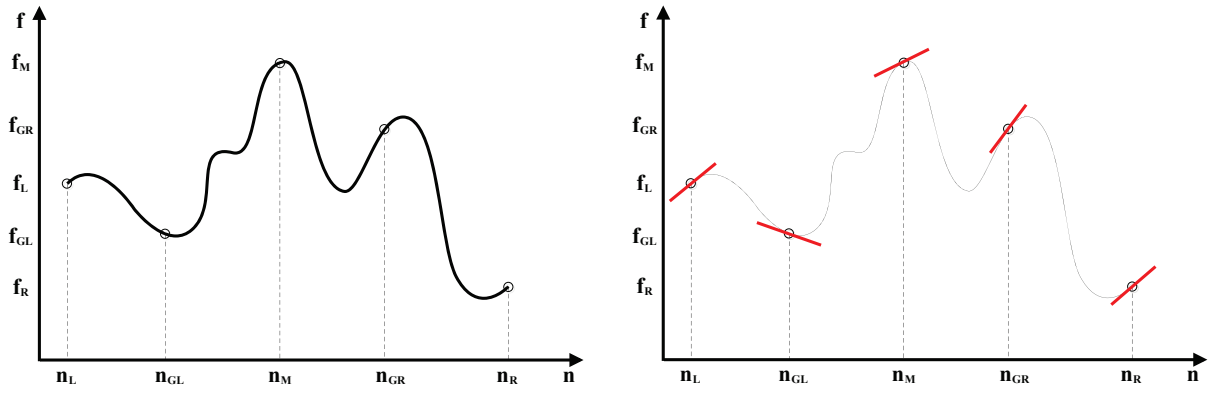

(a) Physical flux

(b) CEN-LLF

(c) CEN-DW

(d) CEN-MDW

Figure 3: Approximation of one wave speed for central schemes

where subscript $j+1/2$ is omitted for brevity. In equations (22), $\phi(r^+)$ and $\phi(r^-)$ are the slope limiters for which r^+ and r^- are defined as

$$r^+ = \frac{n_j - n_{j-1}}{n_{j+1} - n_j}, \tag{23a}$$

$$r^- = \frac{n_{j+2} - n_{j+1}}{n_{j+1} - n_j}. \tag{23b}$$

In order to have TVD properties like monotonicity preservation in a high-order scheme, non-linear slope limiters may be used to restrict the variable gradients within each cell. Here, the following limiters are used (Van Leer, 1977; Sweby, 1984)

minmod (mm) $$\phi_{mm}(r) = \min(r, 1), \tag{24a}$$

van Leer (vl) $$\phi_{vl}(r) = \frac{1+|r|}{1+r}, \tag{24b}$$

monotonized central (mc) $$\phi_{mc}(r) = \max\left\{0, \min\left[2, \min\left(2r, \frac{r+1}{2}\right)\right]\right\}, \tag{24c}$$

for $r > 0$, and $\phi = 0$ for $r \leqslant 0$. It should be noted that when $r = 0$, the second-order piecewise linear solution reduces to the first-order piecewise constant solution.

4.11.2 WENO Reconstruction

In order to use the WENO high-order schemes, n_L and n_R should be reconstructed by a specific polynomial. To increase the accuracy of reconstruction more and more terms should be added to this polynomial. For a second order reconstruction, the procedure reads (Qiu and Shu, 2003)

$$n_L = w_0\left(\frac{1}{2}n_j + \frac{1}{2}n_{j+1}\right) + w_1\left(-\frac{1}{2}n_{j-1} + \frac{3}{2}n_j\right), \tag{25a}$$

and

$$n_R = w_2\left(\frac{1}{2}n_j + \frac{1}{2}n_{j+1}\right) + w_3\left(-\frac{1}{2}n_{j+2} + \frac{3}{2}n_{j+1}\right), \tag{25b}$$

for interface $j+1/2$, where w_0 to w_3 are weight functions that depend on nj, $nj \pm 1$, and $nj \pm 2$ as defined in (Qiu and Shu, 2003).

4.11.3 Characteristic Reconstruction

The reconstruction procedures described above, can be applied to either primitive (original) or characteristic (transformed) sets of variables. Implementing primitive reconstruction, as discussed before, is simple and computationally efficient. On the other hand, using characteristic reconstruction provides better resolution but comes with higher computational cost. The procedure for the latter option is relatively straightforward and contains two transformations together with one typical reconstruction. First, a characteristic decomposition should be performed to produce transformed variables from primitive ones as $\mathbf{w} = \mathbf{R}^{-1}\mathbf{n}$, where $\mathbf{R}$ is defined in equation (11). This transformation should be applied to all primitive variables of the stencil. Then, the same procedure of either MUSCL or WENO reconstruction is used to find $\mathbf{w}_L$ and $\mathbf{w}_R$ from the transformed variables. Finally, an inverse transformation $\mathbf{n} = \mathbf{R}\mathbf{w}$ is applied to retrieve $\mathbf{n}_L$ and $\mathbf{n}_R$.

4.12 Correction for Stagnation and Singular Points

When upwind decomposition-based schemes, i.e., UPW-FLX, UPW-VAR, and UPW-ROE, are used there is a possibility that the numerical scheme produce unphysical entropy violating solutions whenever an eigenvalue associated to a genuinely non-linear expansion (rarefaction) wave reaches

stagnation point, i.e., $\lambda_L \leq \lambda = 0 \leq \lambda_R$. To force the solution to satisfy entropy condition, an entropy correction may be used. Harten's entropy correction can be used for this purpose (Harten and Hyman, 1983)

$$|\lambda| = \begin{cases} \dfrac{\lambda^2 + \varepsilon^2}{2\varepsilon} & |\lambda| < \varepsilon, \\ |\lambda| & |\lambda| \geq \varepsilon, \end{cases} \tag{26}$$

where the tuning parameter ε must be optimized based on the wave speeds of the problem (Kermani and Plett, 2001). In (Moshiri et al., 2013) an approximate relation was given to determine ε for multiphase flows in porous media. Higher values of ε means higher diffusion, while for lower values, non-physical solutions may appear. When decomposition schemes of (11), (12), and (13) are used, this correction is usually applied component-wise, i.e., wave by wave for $|\lambda| \equiv |\lambda_i|$ where $i = 1, 2, \cdots, n_c$. Moreover, the correction (26) can be used along with the CEN-DW one-wave speed of (18) whenever the rare case $(\mathbf{f}_R - \mathbf{f}_L) = 0$ corresponding to $(\mathbf{n}_R - \mathbf{n}_L) \neq 0$ occurs.

Beside correction at stagnation points, another procedure is needed in decomposition-based schemes whenever eigenvector deficiency, i.e. lose of strict hyperbolicity, occurs. In such cases, the relatively complicated procedure of High-Order Godunov (HOG) (Bell et al., 1989) may be used. Another approach for entropy correction was suggested in (Edwards, 2010) which uses CEN-LLF scheme in the problematic points. This entropy fix has the advantage of being parameter free which makes it possible to be used in various contexts. Mathematically speaking, one can use (Edwards, 2010)

$$\hat{\mathbf{f}} = \begin{cases} \hat{\mathbf{f}}_{LLF} & \lambda_{kL} \leq 0 \leq \lambda_{kR}, \qquad k = 1, 2, \cdots, n_c, \\ \hat{\mathbf{f}}_{LLF} & \min(|\lambda_i - \lambda_j|) < \epsilon \left(\max_{k=1}^{n_c} |\lambda_k| \right), \qquad i, j, k = 1, 2, \cdots, n_c, \qquad i \neq j \\ \hat{\mathbf{f}}_{original} & \text{otherwise}, \end{cases} \tag{27}$$

where numerical experiences show that $\epsilon = 0.01$ is a reasonable choice which is already introduced in Table 3. The first line in (27) refers to stagnation points while the second line deals with the umbilic points where eigenvector deficiency may occur as a consequence of equal eigenvalues.

Using CEN-LLF flux in (27) makes this procedure expensive since it requires the computation of several eigen-structures at each face. Here, it is recommended that the $\hat{\mathbf{f}}_{LLF}$ in the relation (27) is substituted by $\hat{\mathbf{f}}_{MDW}$ as defined in (19) to (21).

4.13 Time Integration

To solve the semi-discrete conservation equations (8), two time integration methods are used: 1) first-order forward Euler method and 2) second order Heun method. Defining $\Delta_j \hat{\mathbf{f}}(\mathbf{n}^n) = \hat{\mathbf{f}}^n_{j+1/2} - \hat{\mathbf{f}}^n_{j-1/2}$ and $\Delta \mathbf{n} \equiv \mathbf{n}^{n+1}_j - \mathbf{n}^n_j$, the discrete form of the mass conservation equation is given by

$$\Delta \mathbf{n}^{1st} = -\frac{\Delta t}{\phi_i \Delta x} \Delta_j \hat{\mathbf{f}}(\mathbf{n}^n), \tag{28}$$

for the first-order forward Euler method, and

$$\Delta \mathbf{n}^{2nd} = -\frac{\Delta t}{\phi_i \Delta x} \left[\frac{1}{2} \Delta_j \hat{\mathbf{f}}(\mathbf{n}^n) + \frac{1}{2} \Delta_j \hat{\mathbf{f}}(\mathbf{n}^n + \Delta \mathbf{n}^{1st}) \right], \tag{29}$$

for the second order Heun method.

The stability of the numerical method is determined by setting an upper limit on the Courant-Friedrichs-Lewy (CFL) number defined as

$$\text{CFL} = \frac{\lambda^{\max} \Delta t}{\Delta x}, \tag{30}$$

where $\lambda^{\max}$ is the global maximum wave speed in the solution, i.e.,

$$\lambda^{\max} = \begin{cases} \max\limits_{i=1}^{n_c} |\lambda_i| & \text{for upwind and HLL schemes,} \\ |\lambda_{CEN}| & \text{for central schemes,} \end{cases} \tag{31}$$

Numerical experiences show that whenever second order time integration method is used, a larger value can be assigned to CFL. It should be noted that, the choice of reconstruction methods and slope limiters affects the stability of the numerical schemes.

5 Results

In order to demonstrate the accuracy and computational performance of numerical schemes and procedures presented in this paper, flow of a multi-component multi-phase fluid in a typical one-dimensional reservoir core as shown in Figure 4 is studied. The dip angle θ can vary between $\frac{-\pi}{2}$ and $\frac{\pi}{2}$.

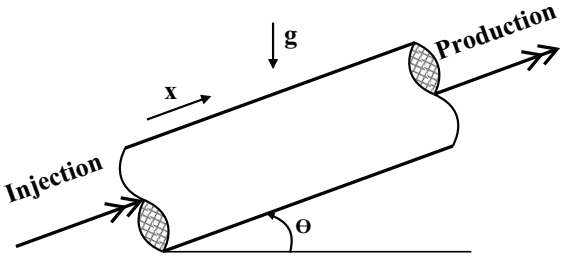

Figure 4: Schematic of reservoir

5.1 No Volume Change on Mixing Test Case

In this section, compositional flow of a five-component two-phase fluid is studied. In order to compare the numerical schemes presented in this paper, the problem is simplified so that only the hyperbolic part of the compositional equations needs to be solved. To this end, it is necessary to set a predefined total velocity over the entire domain. From a physical point of view, if the displacing pressure is high enough the volumes of components do not change when transferring between liquid and vapor phases, i.e. the so-called No Volume Change on Mixing (NVCM) assumption is valid. In such cases, the total velocity becomes independent of pressure (Orr, 2005); hence, the pressure equation is eliminated and a constant pressure can be assigned to the entire domain at all times. Moreover, the NVCM assumption makes it possible to utilize the Method Of Characteristics (MOC) to obtain analytical solutions as described in (Dindoruk, 1992; Orr, 2005). Furthermore, in this test case, the equilibrium ratios, i.e. the ratios of components mole fractions in vapor phase to liquid phase, are assumed to be constant. Physically speaking, if the temperature, pressure, and composition of the two phase system is such that the critical point does not appear in the solution, the equilibrium ratios, i.e. K-values, depend weakly on composition and this dependency can be eliminated, hence the K-values can be assumed constant. The latter assumption has the advantage of eliminating need for EOS calculations, hence making the formulation independent of EOS parameters. For more information on the formulation and the analytical solution of this problem, the reader is referred to (Dindoruk, 1992; Orr, 2005).

The problem consists of injection of pure CO_2 gas into a reservoir initially filled with a mixture of C_1, C_4, C_{10}, and C_{16} in liquid phase. The problem properties together with its initial and injection conditions are given in Table 4. In Figure 5 the computed vapor phase saturation are compared to MOC solution of (Dindoruk, 1992) for various grid sizes while CFL is 0.7. In this figure, the first order UPW-ROE scheme together with Euler forward time integration method are

Table 4: Properties of two-phase NVCM test case

Components	CO_2	C_1	C_4	C_{10}	C_{16}
Injection mole fraction [-]	1.00	0.00	0.00	0.00	0.00
Initial mole fraction [-]	0.00	0.25	0.25	0.25	0.25
Equilibrium ratio [-]	1.50	2.80	0.40	0.20	0.01
Relative permeability [-]	$k_r^\alpha = (s^\alpha)^2$				
Viscosity ratio [-]	$\frac{\mu^l}{\mu^v} = 1$				

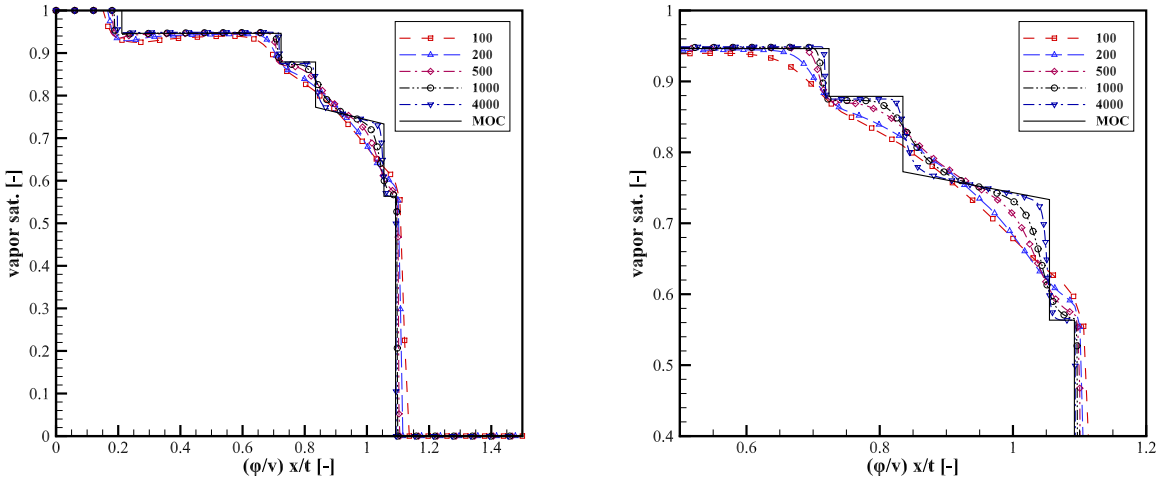

(a) Saturation of vapor phase

(b) Saturation of vapor phase in enlarged domain

Figure 5: Result of vapor phase saturation using UPW-ROE scheme

used and a small portion of domain is magnified in Figure 5b to allows a better distinction between different profiles. The profiles are depicted with respect to dimensionless similarity variable $\frac{\phi}{v^{tot}}\frac{x}{t}$ so that the profiles remain unchanged as the solution marches in time. Theoretically, the total velocity v^{tot} and length of reservoir can be set arbitrarily; however, here, the length of reservoir is set to $l = 1.5$ m and $v^{tot} = 1\frac{\text{m}}{\text{day}}$ and the solution marches to $t_{max} = 1$ day. As it can be seen from Figure 5a, the solution consists of five self-sharpening shocks and the results are in good agreement with that of the MOC. Figure 5a shows convergence to the MOC solution as grid is refined from 100 to 4000 computational nodes. Moreover, it can be seen from Figure 5a that, the flow features such as rarefactions, shocks, and discontinuities are captured well using 500 computational nodes, albeit with some amounts of numerical dissipation. Other schemes exhibit somewhat similar convergence behavior which are not showed here.

In Figure 6 the results of C_1 overall mole fraction are shown for various first order numerical schemes using 100 to 1000 computational nodes while CFL is 0.7. Hereafter, the results are to be compared with a fine solution obtained using the UPW-ROE scheme with 4000 computational nodes which is already shown to match the MOC solution in Figure 5. For the sake of clarity, only a small part of computational domain is shown in Figure 6. Figures 6a and 6b indicate that, HLL and upwind schemes, i.e., UPW-VAR/FLX/ROE, match the analytical solution with higher accuracy while central schemes, i.e., CEN-DW, CEN-MDW, and CEN-LLF, generate larger dissipation. Among latter schemes, CEN-DW and CEN-MDW exhibit better accuracy. Moreover, it is evident that the CEN-LLF scheme have the largest amount of numerical dissipation among the schemes studied here. It is interesting to see that, as the number of computational nodes increases the difference between CEN-DW, and CEN-MDW schemes and upwind scheme becomes

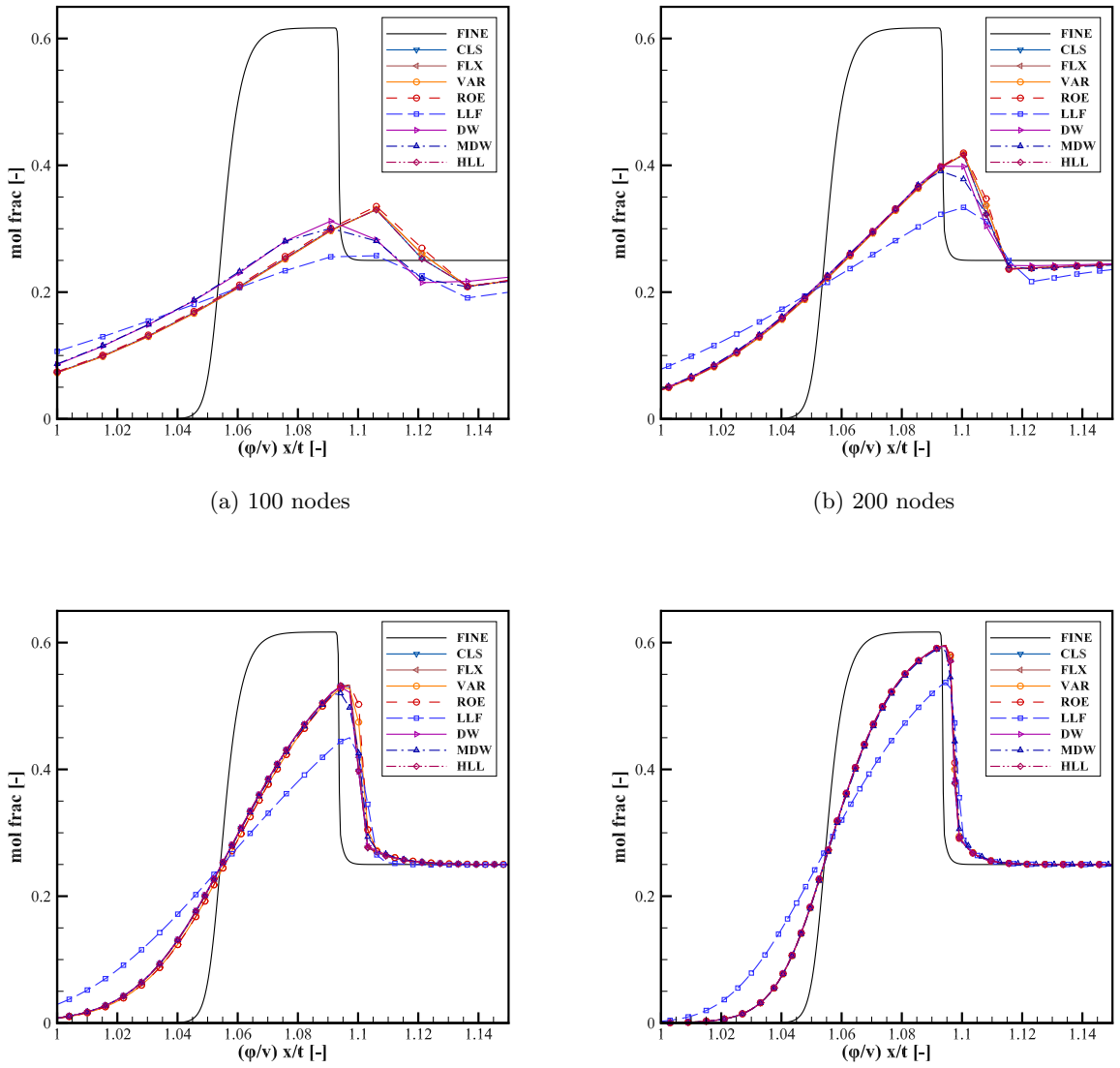

(a) 100 nodes

(b) 200 nodes

(c) 500 nodes in enlarged domain

(d) 1000 nodes

Figure 6: Overall mole fraction of C_1 using first order schemes

less prominent (Figures 6c and 6d). This suggests that CEN-DW and CEN-MDW central schemes can compete well with the more computationally demanding upwind schemes at least in this NVCM example. It should be noted that extremely fine grids are of little interest in practical reservoir simulation studies where a large physical domain should be simulated using limited resources. Hence, in this study the comparisons are made using reasonably fine grids (e.g., 200 or 500 nodes).

While Figures 5 and 6 were dedicated to the first order numerical schemes, Figure 7 shows the results of CO_2 overall mole fraction for various high-order reconstructions using CEN-MDW scheme with CFL = 0.4. It can be seen that both MUSCL and WENO high-order reconstructions dramatically increase the accuracy of results. Figure 7 clearly shows the superiority of the component-wise high-order reconstruction (Figure 7a), over the more computationally demanding characteristic reconstruction (Figure 7b). This behavior does not change when either of MUSCL or WENO method is used. Figure 8 compares the effect of various high order reconstructions on UPW-ROE and CEN-MDW schemes with CFL = 0.4. It is inferred from latter figure that the high order reconstruction increase the accuracy of upwind and central schemes in a similar way. In Figures 7 and 8, the MUSCL method utilizes the minmod limiter; however, using other limiters

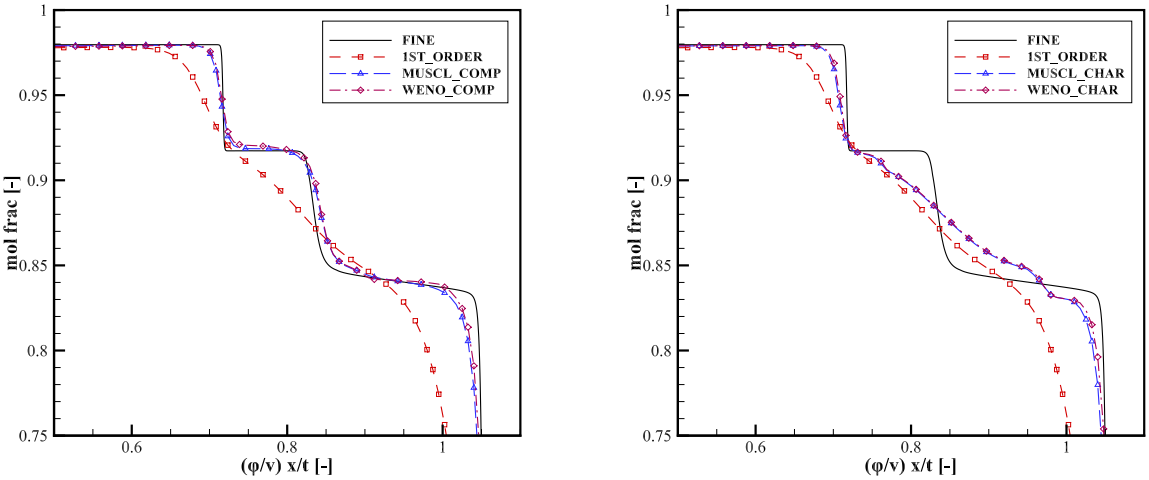

(a) Component-wise reconstruction

(b) Chracteristic reconstruction

Figure 7: Overall mole fraction of CO_2 for various high order reconstruction schemes and 200 nodes using CEN-MDW scheme

will not change the results considerably.

While all aforementioned figures are utilized forward Euler time integration, Figure 9 shows the effect of time integration method on the stability of solution. In Figures 9a to 9c, the results of C_1 overall mole fraction using high-order UPW-ROE scheme with the first-order forward Euler time integration method is compared to the same result using second order Heun time integration method, for three different CFL numbers. It can be seen from Figure 9 that Heun method allows for using larger CFL numbers, so larger time step size can be utilized whenever Heun method is used. Of course, the superiority of the Heun method is somewhat attenuated by knowing the fact that the latter method is much more computationally demanding.

Figure 10 shows the mathematical and numerical wave speeds of this NVCM system. It can be seen from this figure that while in the single phase region the wave structure is smooth, in two phase region both mathematical and numerical wave speeds show considerable variations. Moreover, there are abrupt changes when transferring between single and two phase regions. The latter phenomena can be ascribed to the huge differences between the properties in single and two phase regions. In the mathematical wave structure (Figure 10a), the sorted wave structure ($\lambda_1 \leq \cdots \leq \lambda_{n_c}$) is shown while in Figure 10b, the so called Buckley-Leverett-type wave speed is depicted which is comprised of segments from λ_2 to λ_5. Moreover, in this figure the position of umbilic points are shown in the two phase region.

Nevertheless, with respect to the numerical wave speeds (Figures 10c to 10e) it is evident that in the two phase region all schemes represent somewhat similar numerical wave speeds with minor differences. In particular, it can be seen that the numerical wave speeds of CEN-MDW and HLL schemes are quite similar while the UPW-ROE scheme shows sharper variations especially in the presence of umbilic points.

It should be noted that, for the upwind schemes, i.e. UPW-VAR/FLX/ROE, where the one-wave speed is not calculated by default in the original formulation, this speed is approximated from numerical flux relations (10) to (13) using a linear least square approach as

$$\lambda = -\frac{\boldsymbol{\beta} \cdot \boldsymbol{\gamma}}{\boldsymbol{\beta} \cdot \boldsymbol{\beta}}, \tag{32}$$

where $\boldsymbol{\gamma} = \hat{\mathbf{f}} - \frac{1}{2}(\mathbf{f}_R + \mathbf{f}_L)$ and $\boldsymbol{\beta} = \frac{1}{2}(\mathbf{n}_R - \mathbf{n}_L)$.

It is also interesting to investigate the computational cost of this five-component compositional

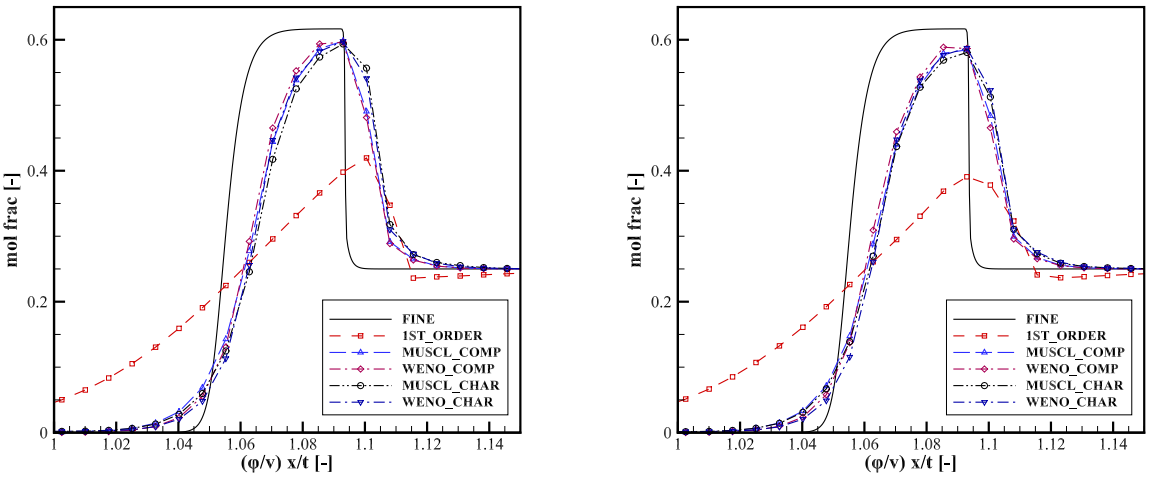

(a) UPW-ROE Scheme

(b) MDW Scheme

Figure 8: Overall mole fraction of C_1 for various high order reconstruction schemes and 200 nodes

problem. Figure 11a compares the overall computational time of various first order numerical schemes while in Figure 11b, the average CPU time is shown for a single interface. It can be seen from Figure 11 that CEN-LLF and HLL have by far the largest CPU times among other schemes while the computational cost of UPW-CLS, CEN-DW, and CEN-MDW are the lowest. To make a better distinction between the computational performances of various schemes, a bar-chart is shown in Figure 11c to compare the CPU times of first order schemes for 2000 computational nodes. It is worth mentioning that, as the number of components increases the gap between computational cost of the latter three and other schemes becomes larger. This is not surprising as the wave structure evaluation becomes more time consuming in large systems.

In Figures 12a and 12b similar diagrams are shown for the case of high order numerical schemes. Here, different high order reconstructions are compared using CEN-MDW scheme. It can be seen from Figures 12a and 12b that, the component-wise MUSCL reconstruction method has the least computational cost while the characteristic-based WENO reconstruction is about twice as more computationally expensive as the former method.

In Figure 13a, error norm of CO_2 mole fraction of is depicted as a function of the number of computational nodes for various first order schemes. The error norms are computed as

$$E = \| \psi - \psi_{exact} \|_2, \tag{33}$$

where ψ is any flow variable and $\| \, . \, \|_2$ indicates second Euclidean norm. Errors are calculated with respect to the 4000 nodes fine solution shown in Figure 5. It can be seen that, CEN-LLF is the least accurate scheme while the error norms of other schemes will eventually converge together as the number of computational nodes increases. Figure 13b shows the error norms of mole fractions of various components using first order CEN-MDW scheme. It is evident that, the C_1 error norm is the largest whereas the CO_2 has the least error with respect to fine solution.

5.2 Typical Two-Phase Compositional Test Case

In this section, a typical one-dimensional compositional problem with volume change and pressure variation is studied. The problem was adopted from (Hoteit and Firoozabadi, 2006) but the boundary conditions are of Dirichlet type, i.e. constant pressure and composition, unlike the original test case that has injection and production wells. In this test case, a gas mixture of C_1 and C_2 is injected into the domain which initially contains a liquid mixture of C_2 and C_3. The required physical data

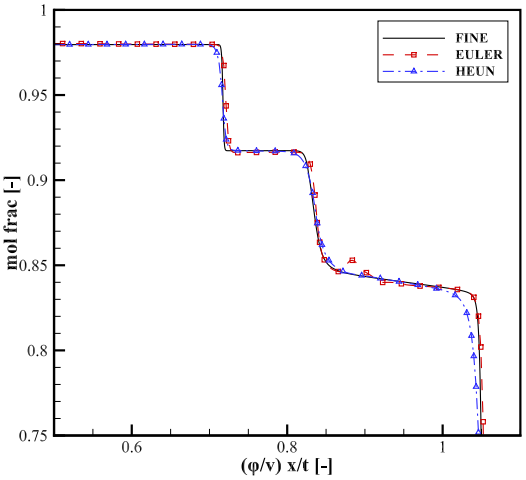

(a) CFL = 0.5

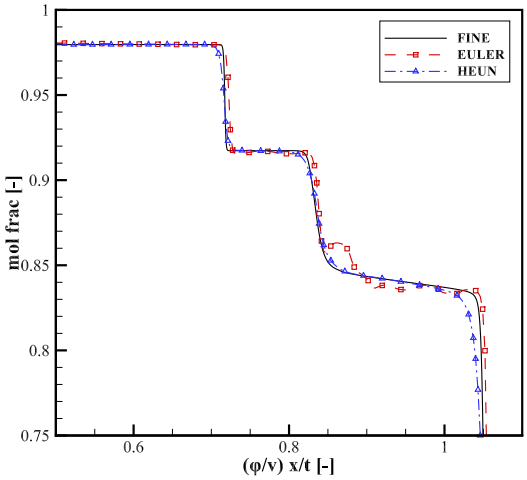

(b) CFL = 0.7

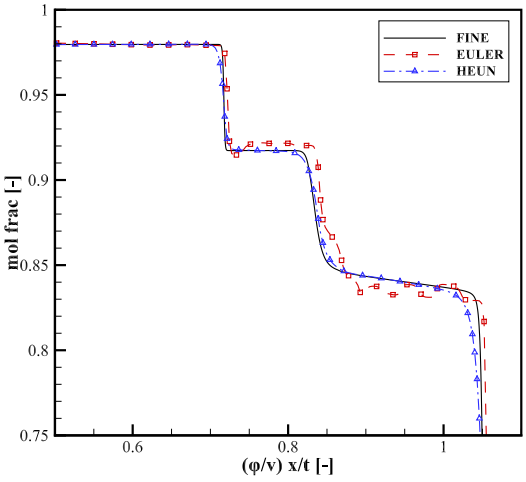

(c) CFL = 0.9

Figure 9: Overall mole fraction of C_1 for different CFL numbers using various time integration methods together with high-order UPW-Roe scheme and 500 nodes

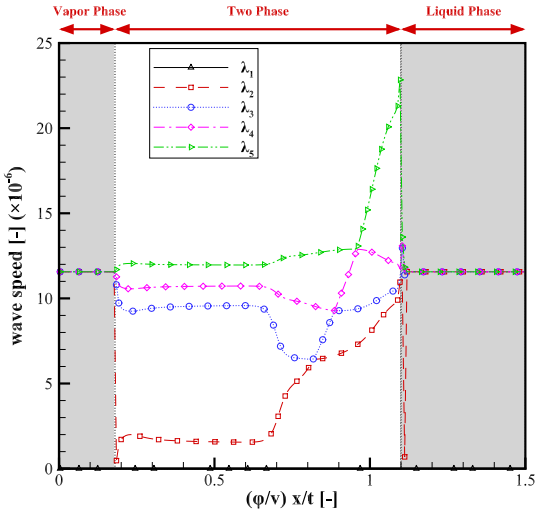

(a) Mathematical wave speeds

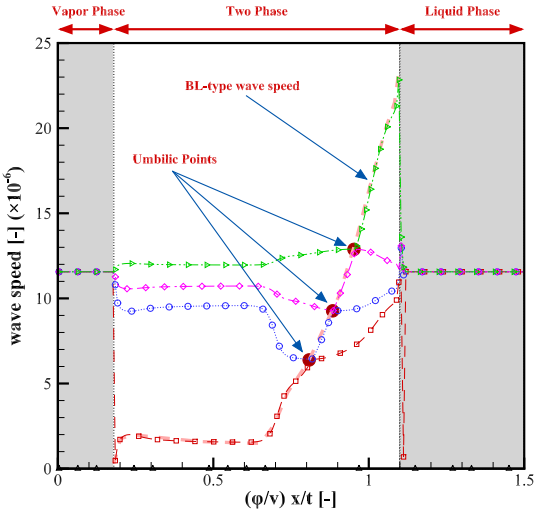

(b) BL-type speed and umbilic points

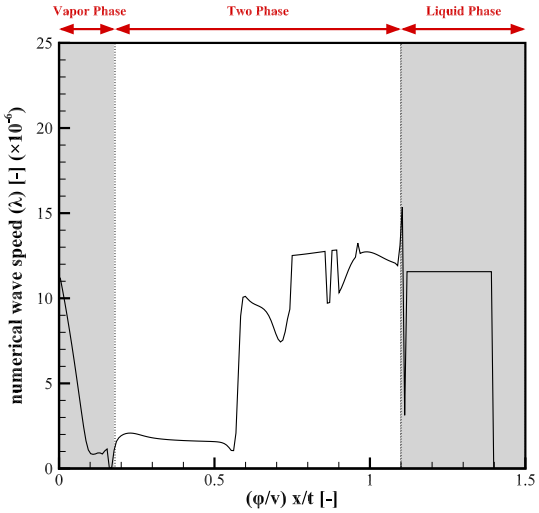

(c) UPW-ROE Scheme

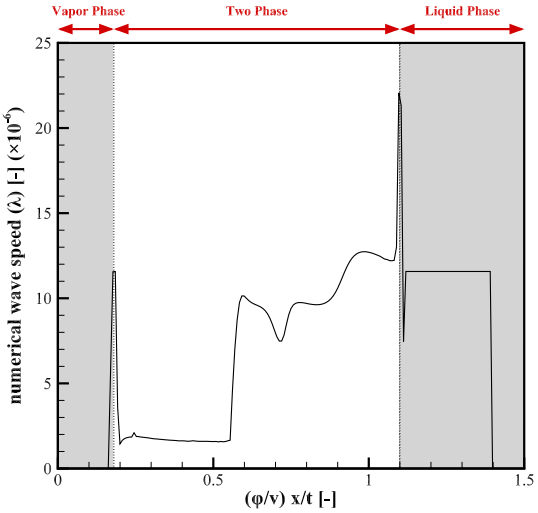

(d) CEN-MDW Scheme

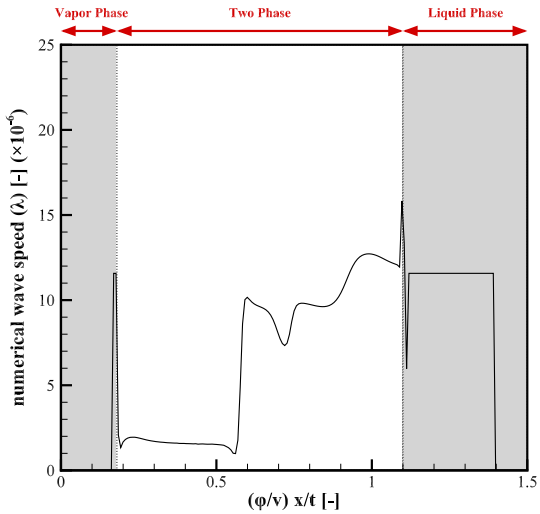

(e) HLL Scheme

Figure 10: Mathematical versus numerical wave speeds using 200 nodes

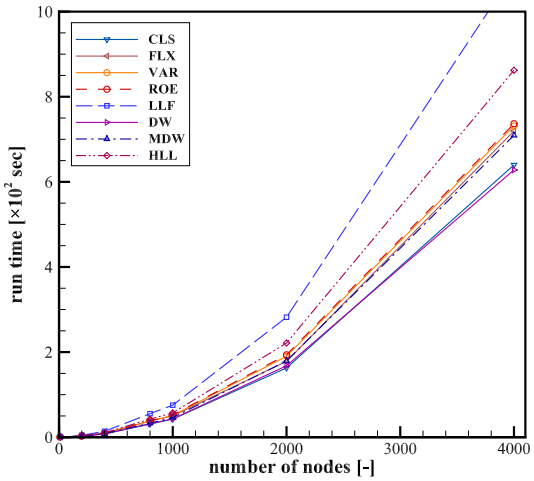

(a) Overall CPU time

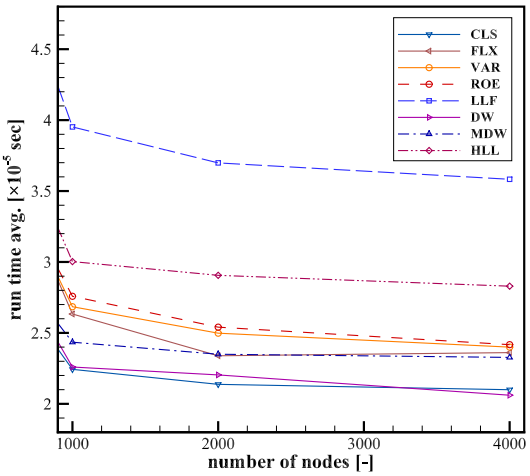

(b) CPU time for single interface in one time step

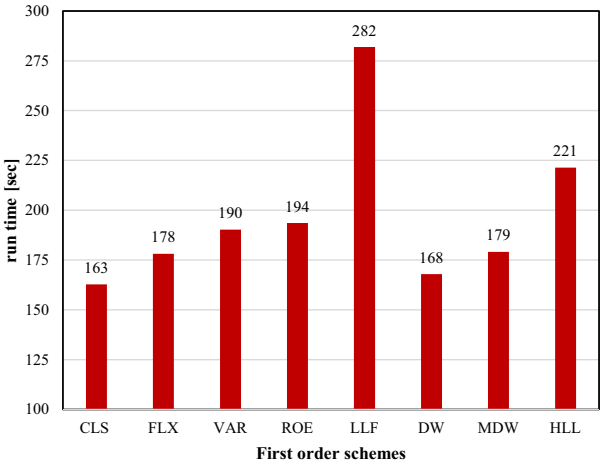

(c) Overall CPU time for 2000 nodes

Figure 11: CPU time for various first order schemes

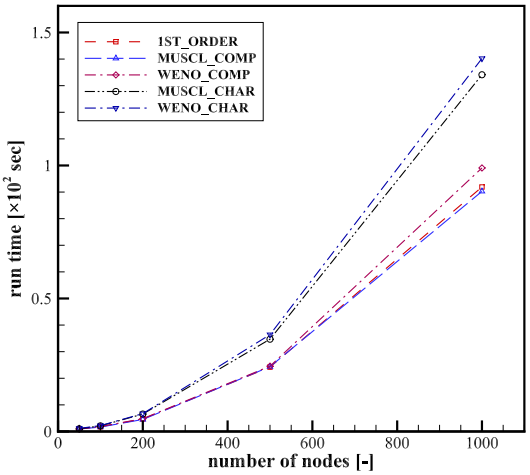

(a) Overall CPU time

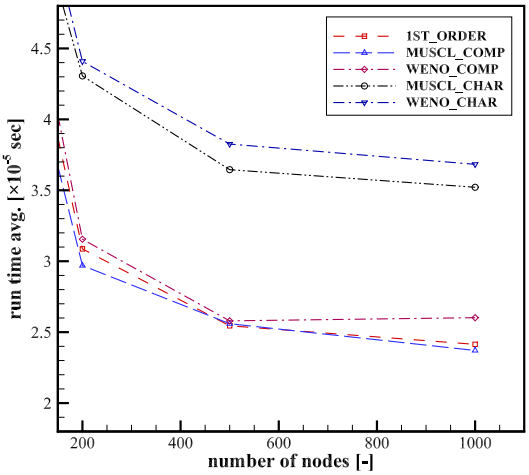

(b) CPU time for single interface in one time step

Figure 12: CPU time for various high order reconstruction using CEN-MDW scheme

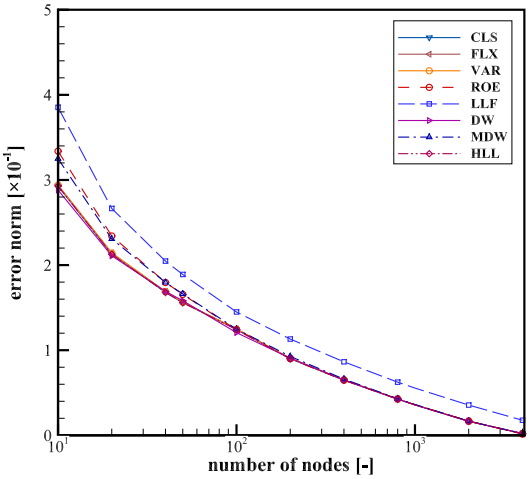

(a) Error norm of CO_2 for various schemes

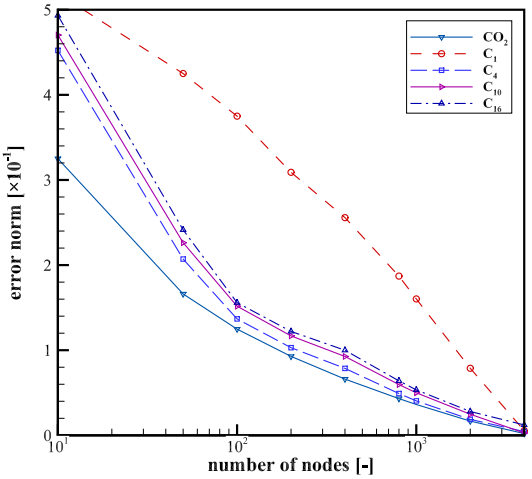

(b) Error norms of various components using CEN-MDW scheme

Figure 13: Error norm for first order schemes

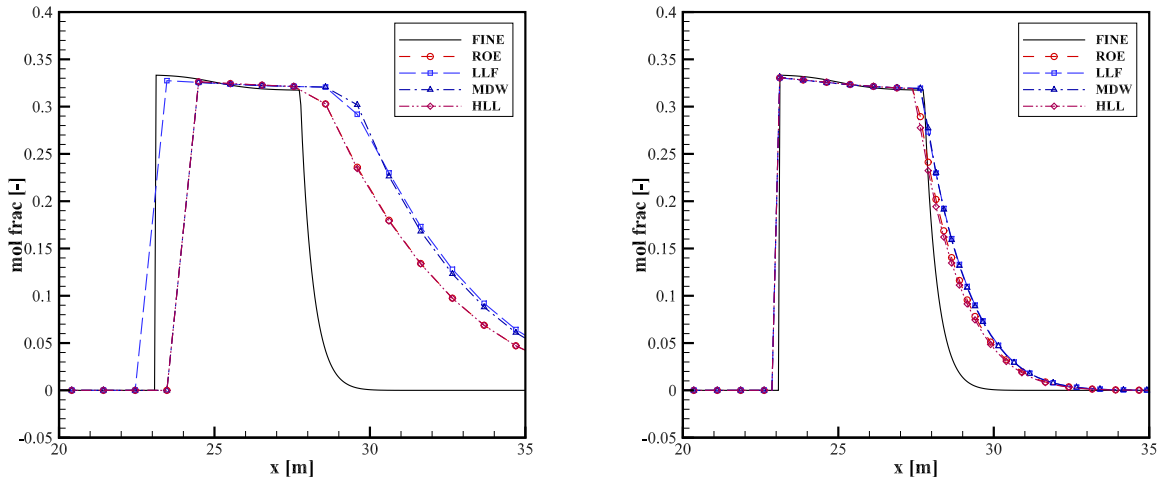

(a) 50 nodes

(b) 200 nodes

Figure 14: C_1 mole fraction in liquid phase using first order schemes

and fluid properties are given in Tables 1 and 2. The length of reservoir is 50 meters and all results are shown after 186 days of injection which is equivalent to 0.51 pore volume injection as described in (Hoteit and Firoozabadi, 2006).

Results of C_1 mole fraction in liquid phase are shown in Figure 14, for various first order numerical schemes using 50 and 200 computational nodes. The CFL is set to 0.7 and the reference solution is obtained using a first order scheme and a fine grid with 5000 nodes. It can be seen from Figure 14 that the UPW-ROE and HLL schemes produce almost the same results while CEN-LLF and CEN-MDW resemble each others. This behavior remains the same for other grid sizes and numerical results shows that all schemes produce grid independent solutions for 500 cells or more.

Figure 15 compares the one-wave speed of selected numerical schemes against eigenvalues (wave speeds) of the hyperbolic system. In fact, this figure shows the connection between mathematical structure of the hyperbolic system and the numerical scheme. Different phase regions are displayed in this figure. In the single phase region, as already shown in (Trangenstein and Bell, 1989), there are two equal wave speeds, whereas in the two phase region, there is Buckley-Leverett speed together with component particle speed (Trangenstein and Bell, 1989). This is in accordance with the wave structure of NVCM system as depicted in Figure 10. The wave speeds change considerably when crossing the two-phase region. These changes are greater near the boundaries of the two-phase region, especially at bubble point. It is evident from Figure 15 that the smallest wave speed is always zero which is an indication of a linearly degenerate system.

It can be seen from Figure 15 that, the one-wave speed of upwind schemes is zero in single phase regions which indicates zero numerical dissipation in those regions in contrast with central schemes, i.e. CEN-LLF and CEN-DW, where considerable amount of dissipation is added to the solution in single phase regions. As expected, the CEN-LLF wave speed is the highest value at each face whereas CEN-DW wave speed lies between eigenvalues of the system. This explains why CEN-LLF scheme adds more dissipation than CEN-DW in those regions. Among other schemes, CEN-DW has the smallest one-wave speed while CEN-LLF has the largest peaks hence highest numerical dissipation. Because of the similarity between two formulations (13) and (11), the behavior of UPW-ROE and UPW-FLX are almost the same which are not depicted here. It can be seen from Figure 15 that for all numerical schemes the maximum wave speeds occur at the problematic composition states, i.e. umbilic and/or elliptic points. This is due to the fact that all schemes try to handle these problematic points by adding numerical diffusion. Note that the upwind schemes used in this paper utilize CEN-MDW formulation for flux approximation when facing problematic

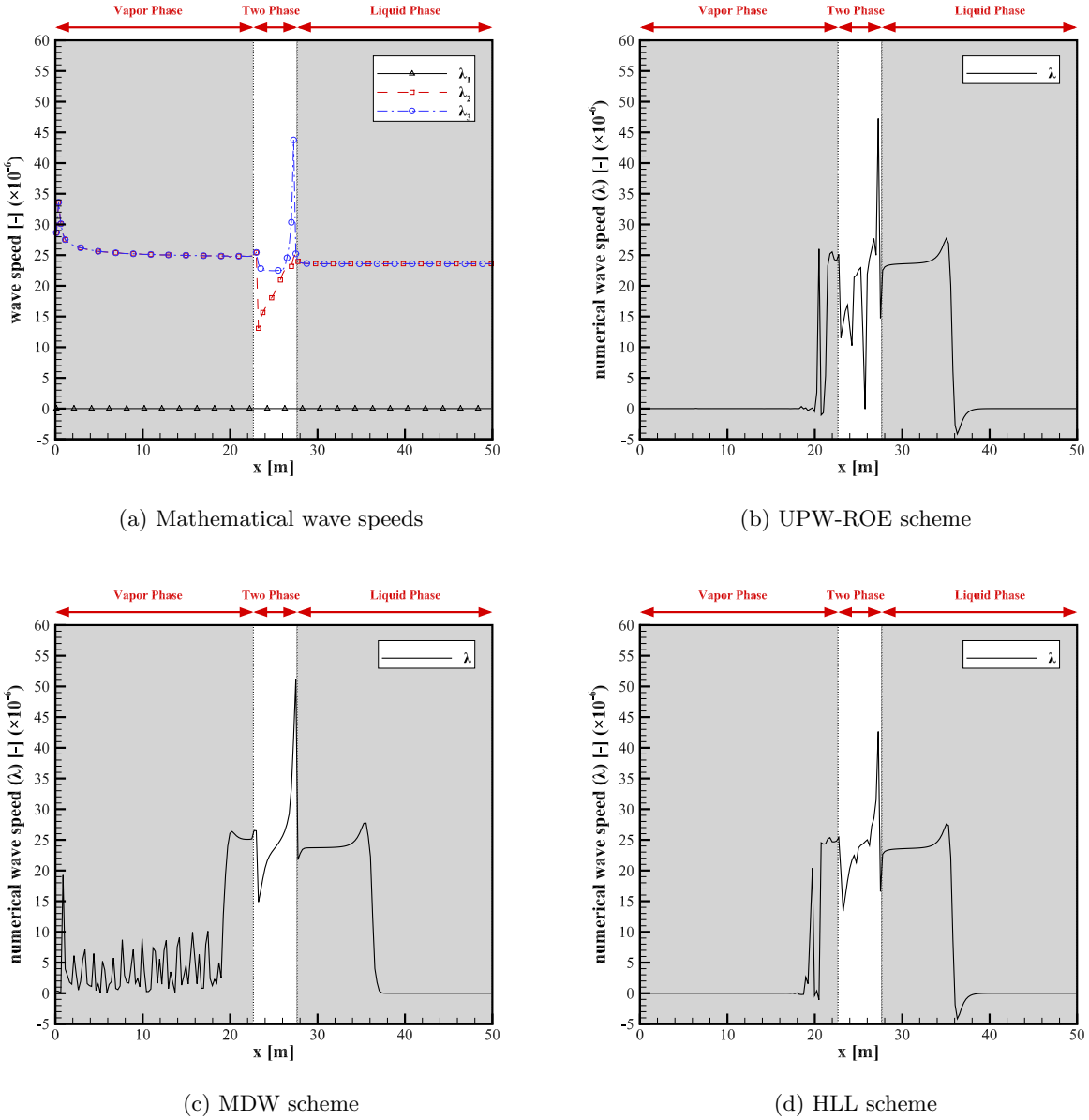

(a) Mathematical wave speeds

(b) UPW-ROE scheme

(c) MDW scheme

(d) HLL scheme

Figure 15: Mathematical and numerical wave speeds for compositional example

points. It can be inferred that the CEN-MDW and UPW-ROE schemes add the least numerical dissipation when facing problematic points while the CEN-LLF scheme adds the highest dissipation in such occasions. Moreover, in this realistic compositional problem, the numerical wave speed of central schemes show spurious oscillations in the single phase regions which are attributed to a few composition states.

Figure 16a shows the composition route for the present problem. This is a path in composition space on which the components travel from injection to production states. It can be seen from Figure 16a that the composition route consists of two nearly straight line segments in single-phase regions, i.e., extensions of initial and injection tie-lines, connected to the ends of a curved segment in the two-phase region which is an indication of non-tie-line path (Dindoruk, 1992). As time marches, this pattern remains almost the same except for slight changes in the two-phase region. The filled circles in this figure indicate compositional states at cell centers which are located equidistantly in the reservoir in a uniform grid. The clustering of these circles in the vicinity of injection, production, and two phase regions indicates that large parts of reservoir lie in these compositional regions.

It should be noted that, since the injection, initial, and production pressures are different, the

phase envelope is not exactly the same for various parts of the reservoir. However, the pressure difference is relatively small, i.e. $\frac{\Delta p}{p_{avg}} \sim 0.01$, and does not noticeably affect the phase behavior, so the ternary phase diagram depicted at mean pressure of injection and production, i.e. $p_{avg} = \frac{p_{inj}+p_{prod}}{2}$, can represent the phase behavior of the entire problem reasonably well.

Figure 16b shows the one-wave speed of CEN-MDW scheme depicted on a ternary phase diagram showing various phase regions. This figure confirms that the largest amount of dissipation belongs to the problematic points in the two phase region. Although Figure 16b may seem different from Figure 15c, especially in the single phase region, they show exactly the same results. This difference is due to the fact that most of the fluctuations in the wave speed in Figure 15c belong to very few composition states in the vapor phase which are very close to each other near the injection state of composition route and virtually disappeared in the phase diagram.

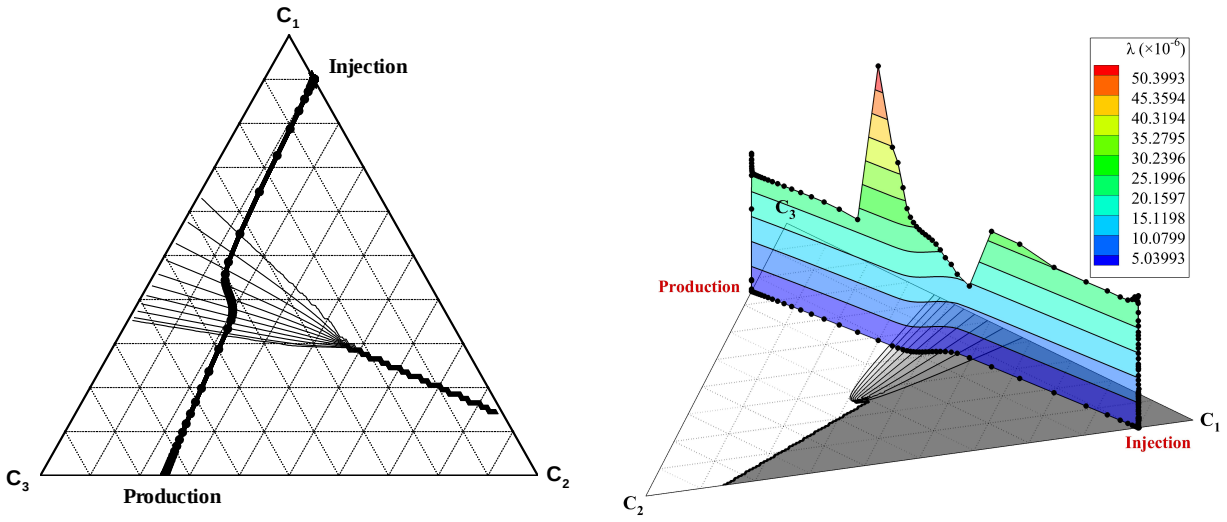

(a) Composition route

(b) MDW wave speed on ternary phase diagram

Figure 16: Results of MDW on ternary phase diagram

It is worth mentioning that, in a typical compositional problem, as the number of components (hence, the number of equations) increases the ratio of computational cost of the hyperbolic part to elliptic part also increases, so most of the CPU time is allocated to solving the composition equations. This mainly occurs due to the evaluation of wave structure which, in turn, requires large matrix computations together with calculation of several physical properties. In fact, the bulk of computational time is dedicated to the evaluation of thermodynamic equilibrium state which is accomplished by iterative routines such as stability analysis and flash calculations as discussed in Appendices A and A.1.

5.3 Three-Phase Test Case

In order to further investigate the MDW scheme in the presence of more complex flows, a three-phase four-component compositional test case is solved in this section. Here, the NVCM assumption is made and two sets of constant partitioning K-values, namely $K_i^{vl} = \frac{x_i^v}{x_i^l}$ and $K_i^{va} = \frac{x_i^v}{x_i^a}$, are given in Table 5. In this test case, the so-called quarter power mixing rule (LaForce et al., 2006) is used to estimate phase viscosities from pure component viscosities mentioned in Table 5. Relative permeability of phase α is defined as (LaForce et al., 2006)

$$k_r^\alpha = \begin{cases} 0 & \bar{s}^\alpha < 0, \\ k_{r0}^\alpha (\bar{s}^\alpha)^{\beta^\alpha} & 0 \le \bar{s}^\alpha \le 1, \\ k_{r0}^\alpha & 1 < \bar{s}^\alpha, \end{cases} \tag{34}$$

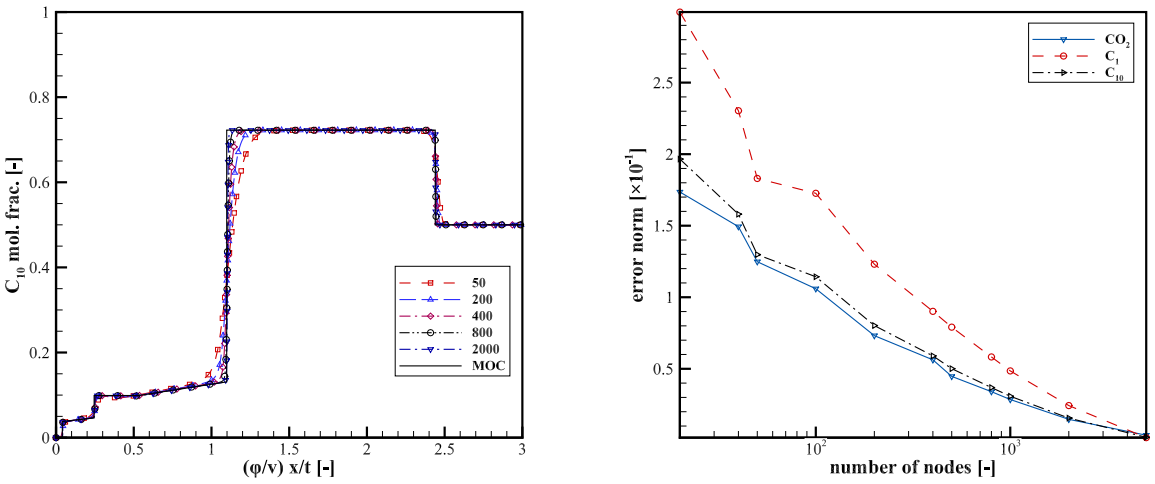

(a) C_{10} mole fraction

(b) Error norms of components

Figure 17: Result of three-phase four-component problem using MDW scheme at PVI=0.333

in which $\overline{s}^{\alpha} = \frac{s^{\alpha} - s_0^{\alpha}}{1 - \sum_{\gamma=1}^{n_p} s_0^{\gamma}}$ and the parameters k_{r0}^{α}, s_0^{α}, and β^{α} are given in Table 6 for all three phases $\alpha = l$, v, and a. The procedures for estimation of fluid properties are briefly stated in Appendix A; for further information, the reader is referred to (LaForce and Johns, 2005; LaForce et al., 2006, 2008a).

The problem consists of injection of CO_2 and H_2O into a reservoir initially saturated with C_1 and C_{10}. The initial and injection compositions are given in Table 5. Dirichlet and Neumann boundary conditions are assigned to the left and right sides of the domain, respectively. CFL is set to 0.5. In Figure 17a, results of C_{10} mole fraction obtained from MDW scheme for various grid sizes are compared to the results of MOC solution shown by (LaForce et al., 2006). Moreover, in Figure 17b the corresponding error norms are presented. It can be seen that, as the number of computational nodes increases, the MDW solution approaches MOC. Moreover, Figures 18a and 18b show the phase saturation profiles at two different PVI in which the phase regions are depicted. In Figure 18c recoveries of C_1 and C_{10} are presented with respect to injected pore volumes. The latter Figure shows a prefect match between analytical and numerical solutions.

Table 5: Fluid properties of three phase problem

Components	CO_2	C_1	H_2O	C_{10}
Injection mole fraction [-]	0.50	0.00	0.50	0.00
Initial mole fraction [-]	0.00	0.50	0.00	0.50
K_i^{vl} [-]	1.5	10.0	2.0	0.005
K_i^{va} [-]	0.1	0.05	50.0	0.001
Pure component viscosity [cP]	0.15076	0.11072	1.0	0.8632

Table 6: Parameters of relative permeability model of three phase problem

Phase	Liquid	Vapor	Aqua
s_0^{α} [-]	0.1	0.05	0.12
β^{α} [-]	2.00	2.00	2.00
k_{r0}^{α} [-]	0.9	1.0	0.85

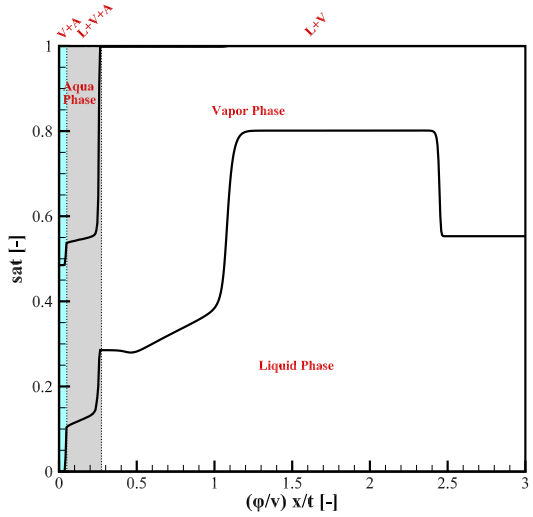

(a) Saturation of phases at PVI=0.333

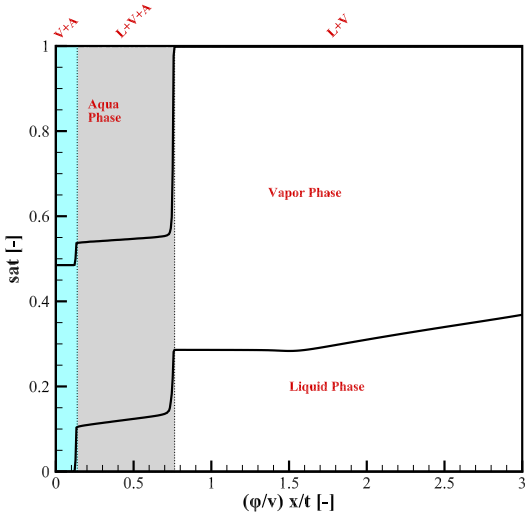

(b) Saturation of phases at PVI=1.00

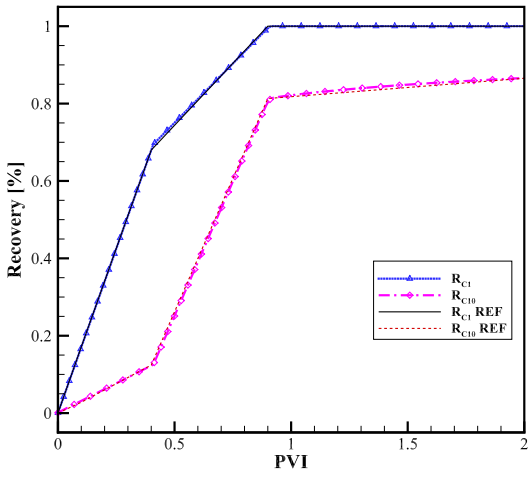

(c) Recoveries of C_1 and C_{10}

Figure 18: Result of three-phase four-component problem using 500 nodes

6 Conclusion

In this paper, several numerical schemes were used to solve hyperbolic system of mass conservation equations of two and three phase compositional model. These include Classical Upwind (UPW-CLS), Flux-based Decomposition Upwind (UPW-FLX), Variable-based Decomposition Upwind (UPW-VAR), Roe-based Decomposition Upwind (UPW-ROE), Local Lax Friedrichs (CEN-LLF), Dominant Wave (CEN-DW) and HLL schemes. A new numerical scheme (CEN-MDW) was proposed which inherits the advantages of both CEN-DW and CEN-LLF schemes. It was shown that the new scheme can compete well with others while maintaining computational cost low.

Despite very low computational cost of CEN-DW, this scheme utilizes only L and R states and neglects the flux variations in between. However, the new CEN-MDW scheme alleviates this deficiency by utilizing several states between L and R while the computational cost does not rise significantly as a consequence of using simple algebraic formula for the wave speed approximation.

The accuracy and computational cost of schemes differ significantly. The characteristic decomposition schemes present better accuracy especially in course grids, but their computational cost is higher in comparison with other schemes when the same grid is used. CEN-LLF scheme has a relatively high computational cost; Moreover, it shows large amount of dissipation due to large wave speed. CEN-DW and CEN-MDW generally require lower computational cost in comparison with other schemes and provide fairly good approximations to wave speed with very low computational cost. It can be suggested that, if the number of equations is low, characteristic decomposition schemes are the best; on the other hand, when facing a problem with a large set of equations (large number of components) the CEN-DW or CEN-MDW schemes are the best choices.

Several options were investigated to produce an upwind flux. While the classical first order upwind scheme is the mainstream approach in commercial simulators, it can be shown that this scheme leads to wrong evaluation of upwind flux when counter-current flow occurs. Among other upwind formulas, the UPW-VAR/FLX/ROE exhibit comparable performances. Given that the UPW-FLX scheme uses the same formulation for upwinding as UPW-VAR except that in the UPW-FLX flux functions are upwinded directly, this can be an indication of preference of flux upwinding over variable upwinding at least in this highly nonlinear problem.

It was shown that all schemes generate maximum numerical dissipation when dealing with problematic points. These points are located mainly in the two phase regions where eigen-values of the system differ from each other. The existence and size of a two phase region, and hence the problematic points, is mainly a function of temperature, pressure, and composition of the problem.

Linear degeneracy of the system was confirmed by means of ternary composition space. The complex wave structure of the two phase system of conservation equations was investigated graphically. It was shown that, the system contains umbilic points in the two phase region while the single phase region has relatively smooth wave structure.

The problem data including the gravity number, relative permeabilities, and viscosity ratios may change in a way that the upwind numerical scheme fails to satisfy entropy condition. In this paper, CEN-MDW flux supersedes the original upwind flux in such points as described in section 4.12.

It was shown that the use of high order variable reconstruction procedures significantly increases the accuracy of solution. However, no significant preference was observed between the second order WENO and MUSCL reconstructions except for relative simplicity of the WENO procedure.

Numerical experiences shows that the CFL number should not exceed 0.5 when high order spatial schemes are used along with the first order forward Euler time integration while in the first order spatial scheme a CFL of 0.7 is acceptable for two-phase problems while for three phase cases CFL should be at most 0.5. Using second order time integration method along with either first or high order spatial scheme significantly increases the stability region to a CFL of 0.9.

Nomenclature

n_c number of components, [-]

n_p number of phases, [-]

s^α saturation of phase α, [-]

μ^α viscosity of phase α, [kg/m.s] or $[\mathrm{ML^{-1}T^{-1}}]$

k_r^α relative permeability of phase α, [-]

ρ^α molar density of phase α, $[\mathrm{kg-mol/m^3}]$ or $[\mathrm{NL^{-3}}]$

ϱ^α mass density of phase α, $[\mathrm{kg/m^3}]$ or $[\mathrm{ML^{-3}}]$

m^α mobility of phase α, [m.s/kg] or $[\mathrm{M^{-1}LT}]$

g gravitational acceleration, $[\mathrm{m/s^2}]$ or $[\mathrm{LT^{-2}}]$

p pressure, [Pa] or $[\mathrm{ML^{-1}T^{-2}}]$

T temperature, [K] or [Θ]

$\mathbf{n}$ vector of component mole numbers, $[\mathrm{kg-mol}]$ or [N]

$\mathbf{z}$ vector of component overall mole fractions, [-]

A mole fractions of aqua phase, [-]

L mole fractions of liquid phase, [-]

V mole fractions of vapor phase, [-]

$\mathbf{x}^\alpha$ vector of component mole fractions in phase α, [-]

$\mathbf{v}^\alpha$ velocity of phase α, [m/s] or $[\mathrm{LT^{-1}}]$

v^{tot} total velocity, [m/s] or $[\mathrm{LT^{-1}}]$

ν_i^{tot} total partial molar volume of ith component, $[\mathrm{m^3/kg-mol}]$ or $[\mathrm{N^{-1}L^3}]$

c_f fluid compressibility, [1/Pa] or $[\mathrm{M^{-1}LT^2}]$

c_r rock compressibility, [1/Pa] or $[\mathrm{M^{-1}LT^2}]$

ϕ porosity, [-]

K absolute permeability, $[\mathrm{m^2}]$ or $[\mathrm{L^2}]$

t time, [s] or [T]

Δt time step size, [s] or [T]

Δx length of grid cell, [m] or [L]

V_j size of jth grid, $[\mathrm{m^3}]$

x length coordinate, [m] or [L]

Z height coordinate, [m] or [L]

θ dip angle, [rad] or $[\theta]$

$\mathbf{f}$ vector of component hyperbolic fluxes, $[\mathrm{kg-mol.m/s}]$ or $[\mathrm{NLT^{-1}}]$

$\hat{\mathbf{f}}$ vector of component numerical fluxes, $[\mathrm{kg-mol.m/s}]$ or $[\mathrm{NLT^{-1}}]$

$\mathbf{q}$ vector of component molar sources/sinks, $[\mathrm{kg-mol/s}]$ or $[\mathrm{NT^{-1}}]$

λ numerical wave speed, [m/s] or $[\mathrm{LT^{-1}}]$

λ_j jth eigen-value of Jacobian matrix, [m/s] or $[\mathrm{LT^{-1}}]$

$\mathbf{\Lambda}$ diagonal matrix of eigenvalues, [m/s] or $[\mathrm{LT^{-1}}]$

$\mathbf{r}_j$ jth right eigen-vector of Jacobian matrix, [-]

$\mathbf{R}$ matrix of right eigenvectors of Jacobian matrix, [m/s] or $[\mathrm{LT^{-1}}]$

ϕ_{mc} monotonized central slope limiter, [-]

ϕ_{mm} minmod slope limiter, [-]

ϕ_{osh} Osher slope limiter, [-]

ϕ_{vl} van Leer slope limiter, [-]

CFL Courant-Friedrichs-Lewy number, [-]

HLL Harten-Lax-van Leer scheme

UPW- Upwind scheme

CEN- Central scheme

CLS Classical Upwind scheme

FLX Flux-based Decomposition Scheme

VAR Variable-based Decomposition Scheme

ROE Roe-based Scheme

LLF Local Lax- Friedrichs scheme

DW Dominant Wave scheme

MDW Modified Dominant Wave scheme

subscripts

i component index

α	phase index	$j \pm 1/2$	interface index
l	liquid phase	L	left high-order state
v	vapor phase	R	right high-order state
j	node index		

References

Acs, G., Doleschall, S., Farkas, E.: General purpose compositional model. SPE Journal **25**(4), 543–553 (1985)

Aziz, K., Settari, A.: Petroleum reservoir simulation. Applied Science Publication (1979)

Bell, J.B., Colella, P., Trangenstein, J.A.: Higher order Godunov methods for general systems of hyperbolic conservation laws. Journal of Computational Physics **82**(2), 362–397 (1989)

Cao, H.: Development of techniques for general purpose simulators. Ph.D. thesis, Stanford (2002)

Chen, W.H., Durlofsky, L.J., Engquist, B., Osher, S.: Minimization of grid orientation effects through use of higher order finite difference methods. SPE Journal **I**(2), 43–52 (1992)

Chen, Z., Huan, G., Ma, Y.: Computational methods for multiphase flows in porous media. SIAM (2006)

Christlieb, A.J., Liu, Y., Tang, Q., Xu, Z.: High order parametrized maximum-principle-preserving and positivity-preserving WENO schemes on unstructured meshes. Journal of Computational Physics **281**, 334–351 (2015). DOI 10.1016/j.jcp.2014.10.029. URL http://dx.doi.org/10.1016/j.jcp.2014.10.029

Coats, K.H.: A note on IMPES and some IMPES-based simulation models. SPE Journal **5**(3), 245–251 (2000)

Conte, S.D., de Boor, C.: Elementary numerical analysis: An algorithmic approach. McGraw-Hill Higher Education (1980)

Danesh, A.: PVT and phase behaviour of petroleum reservoir fluids. Elsevier (1998)

Dicks, E.M.: Higher order godunov black-oil simulations for compressible flow in porous media. Ph.D. thesis, Reading (1993)

Dindoruk, B.: Analytical theory of multiphase mullticomponent displacement in porous media. Ph.D. thesis, Stanford (1992)

Edwards, M.G.: Non-upwind versus upwind schemes for hyperbolic conservation laws in porous media. In: SPE Reservoir Simulation Symposium (2005)

Edwards, M.G.: The dominant wave-capturing flux: A finite-volume scheme without decomposition for systems of hyperbolic conservation laws. Journal of Computational Physics **218**(1), 275–294 (2006). DOI 10.1016/j.jcp.2006.02.005. URL http://linkinghub.elsevier.com/retrieve/pii/S0021999106000817

Edwards, M.G.: Global and local central non-upwind finite volume schemes for hyperbolic conservation laws in porous media. International Journal for Numerical Methods in Fluids **64**(7), 793–811 (2010). DOI 10.1002/fld

Falls, A.H., Schulte, W.M.: Theory of three-component, three-phase displacement in porous media. SPE Reservoir Engineering **7**(3), 377–384 (1992)

Firoozabadi, A.: Thermodynamics of hydrocarbon reservoirs. McGraw-Hill (1999)

Godunov, S.K.: A finite difference method for the numerical computation of discontinuous solutions of the equations of fluid dynamics. Mathematicheskii Sbomik **47**(3), 271–306 (1959)

Guzman, R.E., Fayers, F.J.: Mathematical properties of three-phase flow equations. SPE Journal **2**(3), 291–300 (1997)

Han, C., Sepehrnoori, K., Arbogast, T., Miller, M.A.: A fully implicit, compositional, parallel simulator for IOR processes in fractured reservoirs. SPE Journal pp. 1–12 (2006)

Harten, A., Hyman, J.M.: Self adjusting grid methods for one-dimensional hyperbolic conservation laws. Journal of Computational Physics **269**, 235–269 (1983)

Harten, A., Hyman, J.M., Lax, P.D.: On finite-difference approximations and entropy conditions for shocks. Communications On Pure And Applied Mathematics pp. 297–322 (1976)

Haugen, K.B., Sun, L., Firoozabadi, A.: Three-phase equilibrium calculations for compositional simulation. SPE Journal pp. 26–28 (2007)

Hirsch, C.: Numerical computation of internal and external flows. Volume 1: Fundamentals of computational fluid dynamics. Elsevier (2007)

Holden, L.: On the strict hyperbolicity of the Buckley-Leverett equations for three-phase flow in a porous medium. SIAM Journal on Applied Mathematics **50**(3), 667–682 (1990)

Hoteit, H., Firoozabadi, A.: Compositional modeling by the combined discontinuous Galerkin and mixed methods. SPE Journal **11**(1), 19–34 (2006)

Iranshahr, A., Voskov, D., Tchelepi, H.: Generalized negative-flash method for multiphase multi-component systems. Fluid Phase Equilibria **299**(2), 272–284 (2010)

Isaacson, E., Marchesin, D., Plohr, B.J., Temple, J.B.: The Riemann problem near a hyperbolic singularity: The classification of solutions of quadratic Riemann problems. SIAM Journal on Applied Mathematics **48**(5), 1009–1032 (1988)

Isaacson, E., Marchesin, D., Plohr, B.J., Temple, J.B.: Multiphase flow models with singular Riemann problems. Mat. Apl. Comput **11**(2), 147–166 (1992)

Jessen, K., Wang, Y., Ermakov, P., Zhu, J., Orr, F.M.: Fast, approximate solutions for 1d multi-component gas-injection problems. SPE Journal **6**(4), 442–451 (2001)

Johns, R.T., Orr, F.M.: Miscible gas displacement of multicomponent oils. SPE Journal **1**(1), 39–50 (1996). DOI 10.2118/30798-PA. URL http://www.onepetro.org/doi/10.2118/30798-PA

Juanes, R., Patzek, T.W.: Analytical solution to the Riemann problem of three-phase flow in porous media. Transport in porous media **55**(1), 47–70 (2004a)

Juanes, R., Patzek, T.W.: Three-phase displacement theory: An improved description of relative permeabilities. SPE Journal pp. 1–16 (2004b)

Kermani, M., Plett, E.: Modified entropy correction formula for the Roe scheme. American Institute of Aeronautics and Astronautics pp. 1–11 (2001). DOI 10.2514/6.2001-83. URL http://arc.aiaa.org/doi/abs/10.2514/6.2001-83

Kurganov, A., Tadmor, E.: New high-resolution semi-discrete central schemes for Hamilton-Jacobi equations. Journal of Computational Physics **160**(2), 720–742 (2000). DOI 10.1006/jcph.2000.6485. URL http://linkinghub.elsevier.com/retrieve/pii/S0021999100964854

LaForce, T., Jessen, K., Orr, F.: Four-component gas/water/oil displacements in one dimension: Part i. structure of the conservation law. Transport in Porous Media **71**(2), 199–216 (2008a)

LaForce, T., Jessen, K., Orr, F.M.: Four-component gas/water/oil displacements in one dimension: part ii, example solutions. Transport in Porous Media **72**(1), 83–96 (2008b)

LaForce, T.C., Jessen, K., Orr, F.M.: Analytical solutions for compositional three-phase four-component displacements. SPE Journal (2006)

LaForce, T.C., Johns, R.T.: Composition routes for three-phase partially miscible flow in ternary systems. SPE Journal **10**(2), 161–174 (2005)

Laney, C.B.: Computational gasdynamics. Cambridge University Press (1998)

Lax, P.D.: Hyperbolic systems of conservation laws and the mathematical theory of shock waves. SIAM (1973)

Liu, T.P.: The Riemann problem for general systems of conservation laws. Journal of Differential Equations **18**, 218–234 (1975)

Liu, X., Osher, S.: Convex ENO high order multi-dimensional schemes without field by field decomposition or staggered grids. Journal of computational physics **142**(2), 304–330 (1998)

Liu, Y., Shu, C., Tadmor, E., Zhang, M.: Non-oscillatory hierarchical reconstruction for central and finite volume schemes. Communications in Computational Physics **2**(5), 933–963 (2007)

Lohrenz, J., Bray, B., Clark, C.: Calculating viscosities of reservoir fluids from their compositions. SPE Journal of Petroleum Technology **16**(10), 1171–1176 (1964)

Lyra, P.R.M., Morgan, K.: A review and comparative study of upwind biased schemes for compressible flow computation. Part II: 1-D higher-order schemes. Archives of Computational Methods in Engineering **7**, 19–55 (2000)

Mallison, B.T., Gerritsen, M.G., Jessen, K., Orr, F.M., et al.: High order upwind schemes for two-phase, multicomponent flow. SPE Journal **10**(03), 297–311 (2005)

Marchesin, D., Plohr, B.J.: Wave structure in WAG recovery. SPE Journal pp. 209–219 (2001)

Mccain, W.D.: The Properties of Petroleum Fluids. PennWell (1990)

Michelsen, M.L.: The isothermal flash problem. Part I. Stability. Fluid Phase Equilibria **9**(1), 1–19 (1982a)

Michelsen, M.L.: The isothermal flash problem. Part II. Phase-split calculation. Fluid Phase Equilibria **9**, 21–40 (1982b)

Michelsen, M.L., Mollerup, J., Breil, M.P.: Thermodynamic models: Fundamental & computational aspects. In: Thermodynamic Models: Fundamental & Computational Aspects. Tie-Line Publications (2008)

Moortgat, J., Li, Z., Firoozabadi, A.: Three-phase compositional modeling of CO2 injection by higher-order finite element methods with CPA equation of state for aqueous phase. Water Resources Research **48**(12), 1–21 (2012). DOI 10.1029/2011WR011736. URL http://doi.wiley.com/10.1029/2011WR011736

Moshiri, M., Manzari, M.T., Hannani, S.K., Rasouli, A.: Simulation of multiphase flows in porous media with gravitational effects using dominant wave method. International Journal of Numerical Methods for Heat & Fluid Flow **23**(7), 1204–1224 (2013). DOI 10.1108/HFF-11-2010-0182. URL http://www.emeraldinsight.com/doi/abs/10.1108/HFF-11-2010-0182

Nelson, P.: Rapid phase determination in multiple-phase flash calculations. Computers & chemical engineering **11**(6), 581–591 (1987)

Nessyahu, H., Tadmor, E.: Non-oscillatory central differencing for hyperbolic conservation laws. Journal of Computational Physics **87**(2), 408–463 (1990)

Orr, F.M.: Theory of gas injection processes. Tie-Line Publication (2005)

Pan, H., Firoozabadi, A.: Fast and robust algorithm for compositional modeling: Part II - Two-phase flash computations. SPE Journal **8**(4), 380–391 (2003)

Peng, D.Y., Robinson, D.B.: A new two-constant equation of state. Industrial & Engineering Chemistry Fundamentals **15**(1), 59–64 (1976). DOI 10.1021/i160057a011. URL http://pubs.acs.org/doi/abs/10.1021/i160057a011

Qiu, J., Shu, C.: On the construction, comparison, and local characteristic decomposition for high-order central WENO schemes. Journal of Computational Physics **183**, 187–209 (2002). DOI 10.1006/jcph.2002.7191

Qiu, J., Shu, C.: Finite difference WENO schemes with LaxWendroff-type time discretizations. SIAM Journal on Scientific Computing **24**(6), 2185–2198 (2003)

Redlich, O., Kwong, J.N.S.: On the thermodynamics of solutions: V. An equation of state fugacities of gaseous solutions. Chemical Reviews **44**(1), 233–244 (1949)

Rezaveisi, M.: Improvements in phase behavior modeling for compositional simulation. Ph.D. thesis, The University of Texas at Austin (2015)

Roe, P.L.: Approximate Riemann solvers, parameter vectors, and difference schemes. Journal of Computational Physics **43**(2), 357–372 (1981)

Soave, G.: Equilibrium constants from a modified Redlich-Kwong equation of state. Chemical Engineering Science **27**(6), 1197–1203 (1972)

Sweby, P.K.: High resolution schemes using flux limiters for hyperbolic conservation laws. SIAM Journal on Numerical Analysis **21**(5), 995–1011 (1984)

Tadmor, E.: Numerical viscosity and the entropy condition for conservative difference schemes. Mathematics of Computation **43**(168), 369–381 (1984)

Tadmor, E.: Entropy stability theory for difference approximations of nonlinear conservation laws and related time-dependent problems. Acta Numerica pp. 451–512 (2003). DOI 10.1017/S0962492902000156

Thiele, M.R., Edwards, M.G.: Physically based higher order godunov schemes for compositional simulation. SPE Journal (2001)

Toro, E.F.: Riemann solvers and numerical methods for fluid dynamics: A Practical introduction. Third edn. Springer (2009)

Trangenstein, J.A.: Three-phase flow with gravity. Contemporary Mathematics **100**, 147 (1989)

Trangenstein, J.A.: Numerical solution of hyperbolic partial differential equations. Cambridge University Press (2007)

Trangenstein, J.A., Bell, J.B.: Mathematical structure of compositional reservoir simulation. SIAM Journal on Scientific and Statistical Computing **10**(5), 817 (1989)

Van Leer, B.: Towards the ultimate conservative difference scheme. II. Monotonicity and conservation combined in a second-order scheme. Journal of Computational Physics **14**(4), 361–370 (1974)

Van Leer, B.: Towards the ultimate conservative difference scheme. IV. A new approach to numerical convection. Journal of Computational Physics **23**, 276–299 (1977)

Watts, J.W.: A compositional formulation of the pressure and saturation equations. SPE Reservoir Engineering **1**(3), 243–252 (1986)

Whitson, C.H., Brulé, M.R.: Phase behavior, vol. 20. SPE (2000)

A Fluid Properties and Thermodynamic Equilibrium

In order to determine phase properties, e.g., density ρ^α, viscosity μ^α, and saturation s^α, in a compositional model, thermodynamic (or phase) equilibrium state must be known. A multi-component multi-phase system at specified temperature and pressure is in thermodynamic equilibrium when there is no driving force to transport a component between different phases (Danesh, 1998). In this case, each phase has its own composition, but all phases have the same temperature and pressure. Total mole fraction of components $\mathbf{z} = \mathbf{n}/(\mathbf{e}^T\mathbf{n})$ and mole fraction of components in phase α, $\mathbf{x}^\alpha = \mathbf{n}^\alpha/(\mathbf{e}^T\mathbf{n}^\alpha)$ are defined with respect to $\mathbf{n}$ and $\mathbf{n}^\alpha$ in section 2. Thermodynamic equilibrium state of a multi-component multi-phase system is the state with minimum Gibbs energy. Mathematically speaking $dG(T, p, \mathbf{z}) = 0$, where G represents Gibbs energy (Whitson and Brulé, 2000; Nelson, 1987).

In order to find out how many phases exist in the reservoir, stability analysis (Michelsen, 1982a) should be performed that specifies the number of phases by evaluating different probable single, two or three-phase states. Again, the actual state is the one which has the least Gibbs energy (Whitson and Brulé, 2000).

Whenever more than one phase exist, flash calculation is performed to determine the composition of each phase. For a system with liquid, vapor, and aqua phases, the criterion of thermodynamic equilibrium becomes (Firoozabadi, 1999; Michelsen et al., 2008)

$$f_i^l(T, p, \mathbf{x}^l) = f_i^v(T, p, \mathbf{x}^v) = f_i^a(T, p, \mathbf{x}^a), \qquad i = 1, \cdots, n_c, \tag{A.1}$$

where f_i^α is partial fugacity of component i in phase α.

f_i^α is a complicated non-linear function of T, p, and $\mathbf{x}^\alpha$ which is derived by using Equation Of State (EOS). In order to calculate the fugacity in the flash calculations, the EOS is employed for each phase separately. Various types of EOS may be used to this end, for example (Redlich and Kwong, 1949; Soave, 1972; Peng and Robinson, 1976), among them Peng-Robinson (Peng and Robinson, 1976) is used here for hydrocarbon phases. The latter EOS is a cubic function of phase compressibility factor $Z^\alpha = p/(\rho^\alpha RT)$ where R is the universal gas constant. Consequently, the inputs of flash calculations are T, p, and $\mathbf{z}$; while, the outputs are $\mathbf{x}^\alpha$, and Z^α for $\alpha = l, v, a$. This information is used to estimate the values of ρ^α which, in turn, leads to calculation of phase saturation s^α and relative permeabilities as a function of saturation. In order to calculate phase viscosities μ^α, algorithm of (Lohrenz et al., 1964) is used. Details of these calculations can be found in (Whitson and Brulé, 2000; Michelsen et al., 2008). It should be noted that, the NVCM test cases studied in this paper use constant K-values assumption, hence in this case the stability and flash procedures become independent of EOS (Orr, 2005; LaForce et al., 2006, 2008b).

A.1 Flash Procedure

1. Given the overall composition z_i, $K_i^{lv} = \frac{x_i^l}{x_i^v}$ and $K_i^{av} = \frac{x_i^a}{x_i^v}$ are defined as the ratios of component mole fraction in liquid and aqua phases to vapor phase, respectively. Whenever all three phases, i.e., liquid, vapor, and aqua, are presented simultaneously, the so-called multi-phase Rachford-Rice equation (Michelsen et al., 2008) should be solved iteratively, with an initial guess from stability analysis, to determine the mole fraction of liquid and aqua phases. Mathematically speaking,

$$F_1(L, A) = \sum_{i=1}^{n_c} \frac{z_i(K_i^{lv} - 1)}{1 + L(K_i^{lv} - 1) + A(K_i^{av} - 1)} = 0, \tag{A.2a}$$

$$F_2(L, A) = \sum_{i=1}^{n_c} \frac{z_i(K_i^{av} - 1)}{1 + L(K_i^{lv} - 1) + A(K_i^{av} - 1)} = 0, \tag{A.2b}$$

where, L, V, and A are the mole fractions of liquid, vapor, and aqua phases, respectively.

2. The mole fraction of components in the vapor phase is solved from the overall material balance equation as

$$x_i^v = \frac{z_i}{1 + L(K_i^{lv} - 1) + A(K_i^{av} - 1)}, \qquad i = 1, \cdots, n_c, \tag{A.3}$$

hence, $x_i^l = K_i^{lv} x_i^v$ and $x_i^a = K_i^{av} x_i^v$ for $i = 1, \cdots, n_c$.

3. If composition dependent K-values are used, given the T, p, $\mathbf{x}^l$, $\mathbf{x}^v$, and $\mathbf{x}^a$, EOS is solved for all phases, and the fugacities of each component in each phase are calculated. Finally, the K_i^{lv} and K_i^{av} in step (1) are updated successively as

$$K_i^{lv} = K_i^{lv,old} f_i^v / f_i^l, \tag{A.4a}$$

$$K_i^{av} = K_i^{av,old} f_i^v / f_i^a, \tag{A.4b}$$

until $f_i^l = f_i^v = f_i^a$ within a preset tolerance.

4. If only two phases are present, depending on the type of existing phases, one of the following equations must be solved

$$\text{for liquid-vapor mixture,} \qquad F_1(L, 0) = 0, \tag{A.5a}$$

$$\text{for aqua-vapor mixture,} \qquad F_2(0, A) = 0, \tag{A.5b}$$

$$\text{and for liquid-aqua mixture,} \qquad F_1(L, A) = F_2(L, A). \tag{A.5c}$$

It should be noted that, the properties needed for calculations are given in Tables 2, 4 and 5.